The Theory of Crimp of Textile Fibers

By

Masao HORIO*

(Received April 18, 1964)

The fundamental idea running through this paper is to correlate the crimps of textile fibers with bilateral structure which was found by the author and collaborators, and a series of results obtained by them on this line are reviewed. Section I outlines the study on the crimped rayon staple which gave rise to finding the bilateral structure. Several species of wool fibers are also endowed *a priori* with bilateral structure, which induces the fibers to crimp as shown in Section II. Section III deals with the mathematical analysis of the dynamics of crimp. The ideal form of crimp is the helical spring, which is preferred to the plane zig-zag from the practical point of view. Section IV describes the production of bilateral fibers made up of two components by the "conjugate melt spinning" process. It is important in the processes of treating the filaments and fabrics that the component polymers in each bilateral filament should be kept inseparable. The compatibility of the several pairs of polymers is estimated by the study of epitaxy, as mentioned in Section V. It is shown in Section VI that the chemical similarity between different polymers is also an essential factor to produce strong cohesion. In Section VII, some of the practical data of crimps, such as the diameter of helix and the number of crimps per unit length are shown with several kinds of conjugate-spun fibers as a function of degree of stretching before producing coiling, the conditions of heat treatment and so forth.

SECTION I

Crimped Rayon Staple

The unique and highly esteemed status of wool in the textile field is due largely to its excellent crimp, which is a basic characteristic of wool fibers. The merino wool, which is one of the most valuable fibers in the world, possesses indeed a number of attractive characters, but if it was not endowed with its characteristic fine crimp, all its other virtues would end in nothing. The crimp of staples is the essential factor which, not only makes spinning easy, but imparts very delicious and warm feeling to the yarns and fabrics. In view of its practical importance, research workers in various fields of science and industry have long been interested in the crimp of textile fibers.

* Department of Polymer Chemistry.

Twenty five years ago in the course of studies being made of the development of a new two-bath stretch spinning process of viscose fibers, the formation of finely crimped filaments was discovered by us. Such filaments displayed crimps which were equal to those of the most superior merino wool fibers, as shown in Fig. 1. It was found that such crimps occurred whenever the acid content in the coagulating bath was reduced to a certain degree below that previously employed in practical viscose spinning. At present, about 65% of the rayon staple produced in Japan is the crimped staple manufactured by this process*.

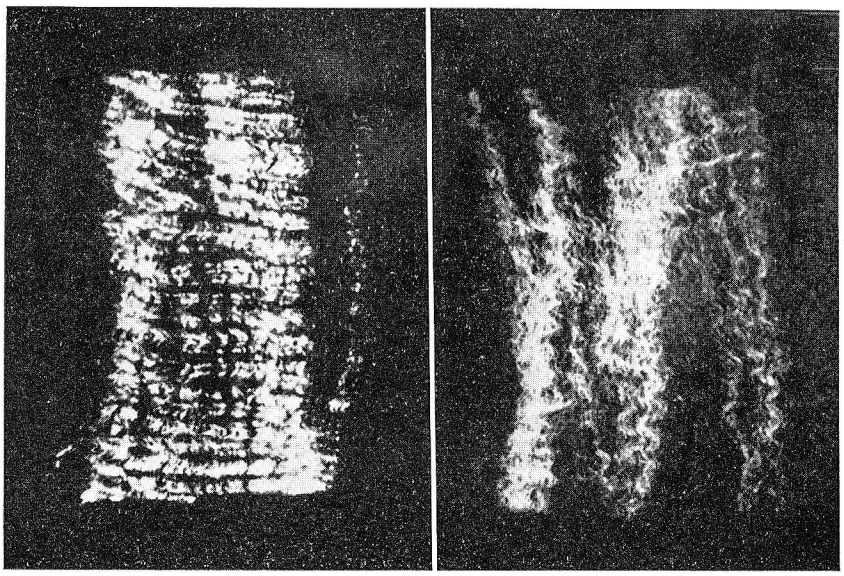

a b

Fig. 1. Crimped rayon staple (a) and merino wool (b). (Magnification ×3.6)

The systematic studies on the morphology of crimped rayon staple revealed that it has a characteristic cross section, which can be separated into two different parts by a boundary line, as shown in Fig. 2, a and b. The appearance of the outline and skin formation above the boundary line, say x-axis, are very different from those below. The upper part A shows finer serrations which are slightly indented, and this part is characterized by a thick skin. On the other hand, the serrations of the lower part B are coarser and deeply notched, and the skin is thinner. The cross section is generally symmetric with respect to an axis which is perpendicular to x-axis, that is $-y$-axis. In other words, the

* The total shipment of rayon staple of Japan in 1963 is 284,000 tons, of which about 186,000 tons are crimped staple.

crimped fiber is compared to the bicomponent filament, which is composed of two different parts combined closely side by side throughout the entire length of the filament. Such a structure we called "bilateral structure". With increasing acid content the cross section becomes more symmetric, as shown in Fig. 2, c–f. Fig. 2, f shows the cross section of the ordinary rayon filament with little crimps.

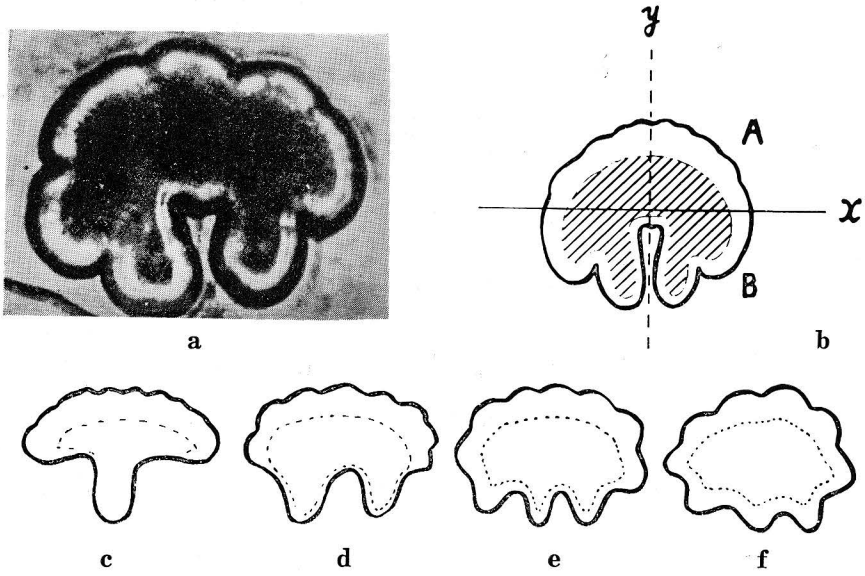

Fig. 2. Cross sections of crimped rayon staple. Cross sections, c–f, are arranged in order of increasing acid content of coagulating bath.

Owing to the different mechanical responses of the two structures, namely A and B, each filament has a pronounced tendency to coil, when the filament is stretched in hot water and then released. Since the side A, having a normal skin, is more elastic than the side B which is provided with a poor skin, the filament coils always in such a manner that the thick-skinned side A faces towards the inside of curvature. Fig. 3 shows a helical coiling of a viscose filament having bilateral structure.

Although a single filament coils in water as shown above, this cannot happen with the individual filaments in a bundle consisting of a huge number of filaments whose directions of coiling are at random. We consider a system consisting of a number of similar filaments with equal bending force of unity in random directions, as shown in Fig. 4, b, then the resultant force vector can be obtained by the statistical calculation of "random walking". The probability function W of the magnitude of the resultant force, p, is expressed as

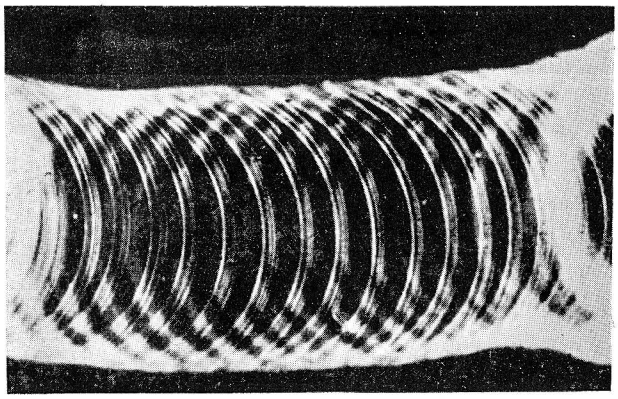

Fig. 3. Helical coil of bilateral rayon filament. ×50

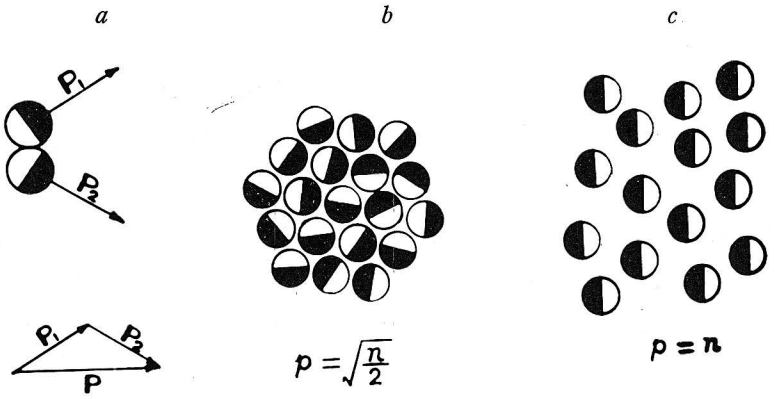

Fig. 4. Bending force produced by multifilament system.

$$W = \frac{2}{n} \cdot p \cdot \exp\left(-\frac{p^2}{n}\right),$$

where n is the total number of filaments.

By differentiating W with respect to p, and putting the result equal to zero, we obtain

$$p = \sqrt{\frac{n}{2}}.$$

This means that in a system composed of n similar filaments having the bending force of unity, the force that is most probably found has a magnitude in the neighborhood of $\sqrt{n/2}$. When the individual forces are in the same

direction, the resultant force should be n. Assuming n to be $2 \cdot 10^6$, which is the magnitude expectable in practical cases, the probable value of the resultant force is only one-thousandth of the value which would be expected when the bending forces of all the filaments are pointed in the same direction. The surface tension of water, which binds each filament close to the other cannot be overcome by so small a force, and the bundle maintains its original straight form, as can be seen in Fig. 5, a.

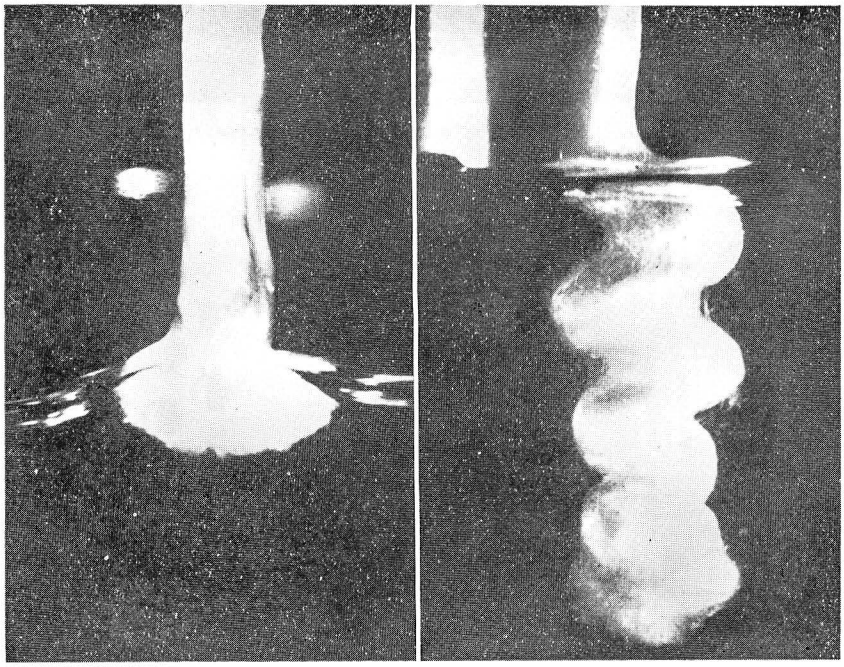

a b

Fig. 5. A bundle of bilateral filaments dipped in water at different depths.

When a bundle is moistened to a greater degree, each individual filament is more widely separated from the other and is capable of moving more freely. It is assumed that a very small inducing force having the magnitude of $1/\overline{n/2}$ is applied in a certain direction during this stage. The most significant factor which decides the behavior of the filaments at this moment is the fact that the twisting rigidity of the filament is much smaller than the modulus of bending. Consequently, each filament is more readily twisted by the external force than it is bent.

All the filaments in the bundle twist in such a manner that their inherent bending character follows the direction of the external influence, and all the

filaments face in the same direction with respect to the bilateral structure. Thus, the bending force increases from $\sqrt{n/2}$ to n, that is — increases thousand times in practice. Fig. 4, c shows this schematically.

The bundle bends, therefore, with the total sum of forces of individual filaments pointing in the same direction. While bending takes place, the resisting force having a magnitude comparable with n is imposed upon the part contiguous to the bending part. In other words, this contiguous region is exposed to an external force pointing in the opposite direction to that of the bending that just occurred. A wave is formed in this manner. Repetition of these processes results in a crimp formation of the bundle, as shown in Fig. 5, b. This explanation applies also to the case where the chip is dipped at once in water. Since the chips are plate-like, a plane wave is formed as shown schematically in Fig. 6. The photomicrograph of the section hatched in Fig. 6 is shown in Fig. 7. It is noticed interestingly in the figure that all the filaments in the chip are facing in the same direction as

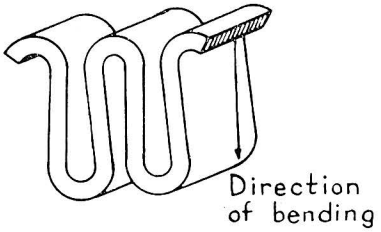

Fig. 6. A waved chip of filaments.

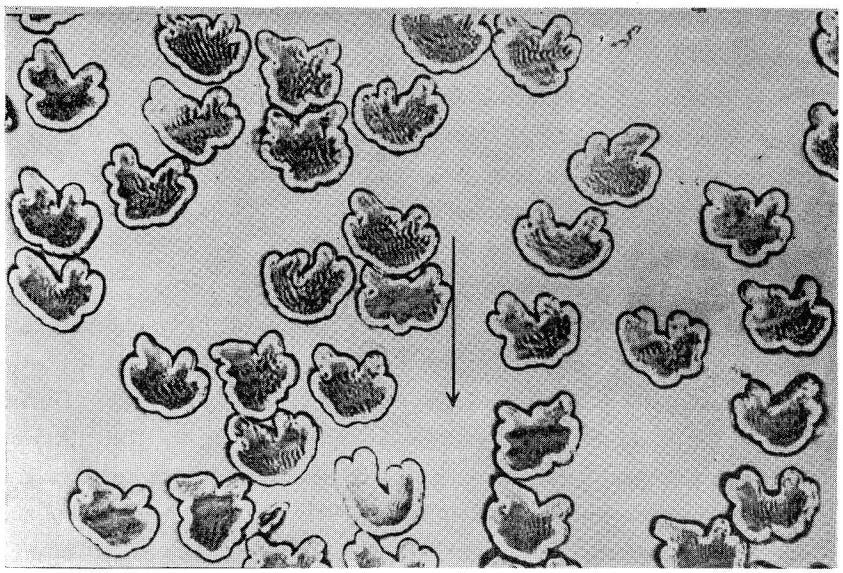

Fig. 7. Photomicrograph of the section of chip hatched in Fig. 6. Arrow shows the direction of bending. All the cross sections are facing in the same direction, that is — the smooth-outlined part towards the direction of bending.

already shown schematically in Fig. 4, c, that is — the smooth-outlined part A points wholly in the direction of the bending.

The next important problem is the origin of producing the bilateral structure in rayon filaments. This can be neatly explained by the consideration of hydrodynamic behavior of bath liquor during the spinning. Thus far, studies on rayon spinning have implied that each viscose filament is uniformly surrounded by the bath liquor throughout its travel in the bath. This could happen only when the spinneret has a single hole at its center and the spinning is performed under no external disturbance of the bath liquor, which is running smoothly together with the filament. In this case, the bilateral structure is not produced.

A spinneret that actually is used in the staple spinning has thousands of holes. Let us consider the flow of bath liquor at P contiguous to the surface of spinneret as shown in Fig. 8. A considerable amount of the bath liquor is

Fig. 8. Flow of bath liquor during the spinning of rayon staple.

continuously carried off by the constant flow of viscose extruded through the holes, and this amount of liquid should be constantly supplied by all means. The consideration of hydrodynamic conditions leads to the conclusion that there is principally only one way to accomplish this liquor supply, that is — the lateral flow as shown by arrows denoted at P. This could be actually demonstrated by several experiments.

As a consequence of the lateral flow each viscose column extruded from the hole of spinneret is attacked by the bath liquor in a manner as shown schematically in Fig. 9. The bath liquor which strikes the apex of a viscose column flows along its surface and leaves it on the opposite side. During this course the liquor is neutralized at the column surface by the alkaline constituents in the viscose. Therefore, the apex is exposed to a relatively strong acid, while the bottom is exposed to a relatively weaker acid. The strength of zinc ion also decreases as the bath liquor flows from apex to bottom. Thus, the structure of filament on both the sides of the boundary line, say x-axis, should be different. This primary reaction gives the filament its inherent character, which cannot be modified fundamentally during the later course of

the spinning process or by any other means. Since the thickness of the liquid film on each column is very small in comparison with the distance between the columns, it can be assumed that almost all the filaments extruded through a spinneret undergo similar reactions.

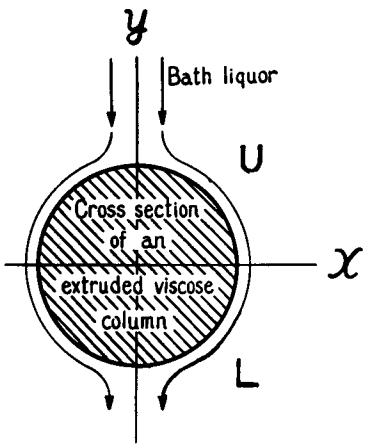

Fig. 9. Flow of bath liquor on a surface of a filament at the point near the spinneret.

The apex is exposed to the normal bath liquor and is subjected to the normal coagulation and regeneration, and there are good reasons for the assumption that the upper part U (Fig. 9) would result in the normally skinned part A of the section sketched in Fig. 2, b. Since the bath liquor is neutralized by degrees and deprived of zinc ions on its way to the bottom, it can happen that the liquor is unable to produce the normal skin at the lower part L of the cross section, when the original acid content of bath liquor is smaller than a certain limit. The thin-skinned part B in Fig. 2, b would have been produced from the lower part L.

As can be deduced from the explanation, the lateral flow and the acid content of bath liquor are the essential factors of producing the bilateral structure. If the acid content is greater than a limit, even the bottom of the viscose column comes in contact with the liquor which is capable of producing normal skin, and consequently the symmetrical cross section is formed.

When the bilaterally structured unfinished filament is stretched in a hot bath, each part responds to it in a different manner depending upon its structure. It is well known that the skin produces a more elastic structure, while the part coagulated to a smaller extent is more thermoplastic. This imparts the coiling property to the filament, in such a manner that the thick-skinned side comes always inside of curvature.

In order that the individual filaments in a chip may point in the same direction with respect to the bilateral structure to form a planar wave, they should be twisted diagonally at every transition from maximum point to minimum point of the wave and *vice versa*, and the twisting should occur alternatively opposite directions.

This is the outline of the theory of crimped rayon staple published in 1953 by us[1].

SECTION II

Crimp of Wool Fibers

No pertinent explanation for the mechanism of crimping of wool fibers had not been found before our theory of the crimping of rayon staple was published. In the course of our studies being made on the theory of crimp it was found that the fundamental principle of crimp formation is quite the same for both the rayon staple and the wool fibers. The motive force of the crimp formation is the coiling nature of fibers coming from the *bilateral structure.*

An analysis of the shape of cross sections of wool fibers does not offer any distinct evidence of bilateral structure, since they are in general oval or circular. However, there are several indications that wool fibers also are typically bilateral in structure, and it is found that the theory we developed with respect to the rayon filament applies exactly to wool fibers[2].

The notable observations made by Ohara[3] should be cited first as an important background of the present theory. He found that the merino fibers are only partially stained by the buffered solutions of several basic dyes and showed that the outside of curvature is stained in a darker tone than the inside. It was also pointed out by him that some of the acid dyes stained preferably the inside of curvature. He thought, however, that the transition region from crest to trough or *vice versa* is stained uniformly. As will be shown below, the wool fibers are bilateral throughout the whole length from root to tip, and the partially staining character exists throughout the entire length of fiber: As in the case of crimped rayon staple, the wool fiber also is twisted diagonally at the transition region from crest to trough of wave, and this would have lead him to the conception of uniform staining.

The partial staining method as presented by Ohara was found to be very useful to reveal the structural asymmetry of wool fibers, which could be correlated with their coiling and crimping nature. Later we[4] could generalize this by a series of experiments, which showed that the occurrence of partial staining is not confined to the specific dyestuffs, but that almost all the dyestuffs which are referred to as basic, acid and substantive dyes stain the wool hair only partially, if the dye bath is buffered so that the pH value does not deviate much from 7 and the dye concentration is adjusted to be so small as from 0.001 to 0.005%.

The experiments were done with sixty five dyestuffs which were picked out of the Colour Index so as to cover all the important types of colors

assigned to the basic, acid and substantive dyes. All the basic dyes stained preferably the outside of curvature, while most of the acid dyes and all the substantive dyes examined stained preferably the inside of curvature. Only a small number of acid dyes such as Formyl Violet (C.I. No. 698)[5], Acid Violet 6B (C.I. No. 697), Acid Violet 3BH (C.I. No. 699), Acid Milling Green 6BN (C.I. No. 667), Alkali Violet 6B (C.I. No. 700) and Xylene Cyanol FF (C.I. No. 715) stained preferably the outside of the curvature, although they are referred to as the acid dyes. These dyes, however, are characterized by the basic nature coming from the basic groups such as alkylamino groups and immonium groups which exceed the sulphonic acid groups in number in the dye molecules, and behave as basic reagents against the cortex[6].

Fig. 10 shows the cross section of wool stained by Methylene Blue. Figs. 11 and 12 show a part of wool fiber stained differentially by Janus Green and Ponceau 2R, respectively.

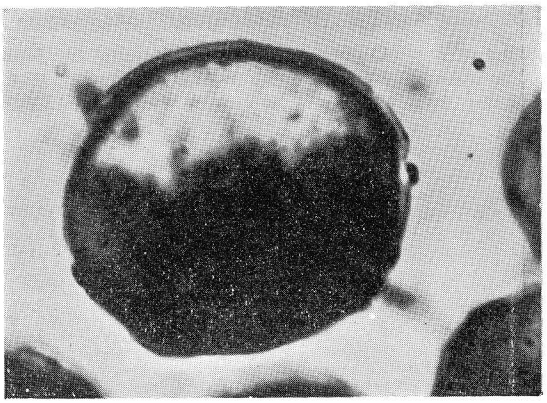

Fig. 10. Differentially stained cross section of a wool fiber by Methylene Blue.

The experiments suggest that the wool hair consists of two different types of cortex, one of which is relatively acidophilic (inside of curvature), and the other is relatively basophilic (outside of curvature). This is demonstrated further by the resistance of both the cortices against reagents such as sodium hydroxide, sulphuric acid, hydrobromic acid[7] and so forth. It has been clearly demonstrated by a number of experiments that the basophilic part is far more sensitive to the alkaline reagents, while the acidophilic part is preferably affected by strong acids.

It is assumed from the results of experiments mentioned above that both the cortices have different chemical constituents. The acidophilic cortex

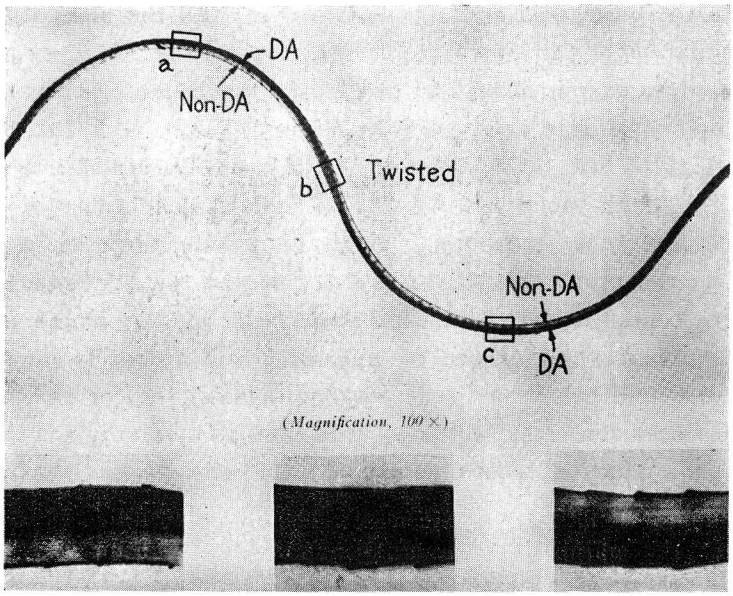

Fig. 11. Part of a wool fiber stained differentially by Janus Green. The outside of curvature is stained in a darker tone, and the fiber is twisted by 180° at the transition point.

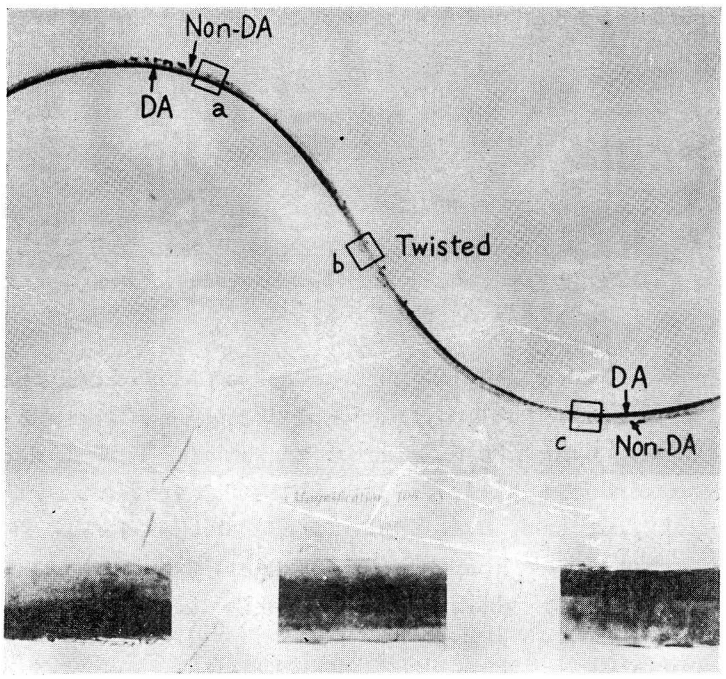

Fig. 12. Part of a wool fiber stained differentially by Ponceau 2R. The inside of curvature is stained in a darker tone, and the fiber is twisted by 180° at the transition point.

is assumed to be richer in the amino acids of basic character, while the basophilic cortex is assumed to be richer in the amino acids of acid character. The isoelectric points of both the cortices were measured in a histochemical way by modifying the method presented by Pischinger[8] and Lison[9]. The apparent isoelectric points of both the cortices are postulated as follows:

	Merino wool	Corriedale wool
Acidophilic cortex	6.75	6.90
Basophilic cortex	5.90	6.15

The result deviates depending upon the conditions of measurements of two types of cortex differing in isoelectric point.

In order to distinguish the two types of cortex from each other, several nomenclatures have been proposed, of which the expressions of "ortho-cortex" and "para-cortex" are now being popularized, but as was discussed in the session of the International Wool Textile Research Conference held in Australia in 1955[10], a more relevant nomenclature is required. Since the two cortices differ in isoelectric point, possibly due to the difference in chemical composition, we propose to call the relatively acidophilic part A-cortex, and the relatively basophilic part "B-cortex". The relation between the two nomenclatures cited above is shown in Fig. 13.

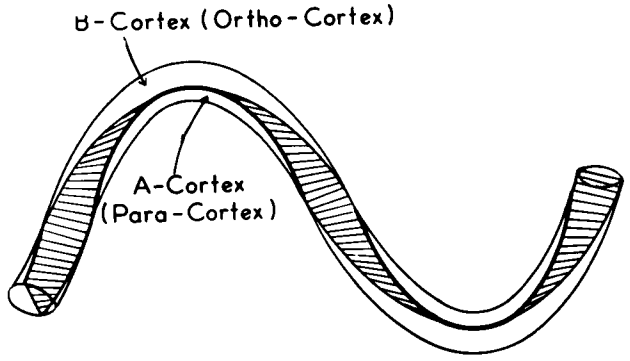

Fig. 13. Nomenclatures to distinguish the two types of cortices.

Besides the partial staining and the difference in resistance to chemicals, the ultraviolet absorption of wool fibers also reveals the bilateral structure. Fig. 14 shows a series of photomicrographs of cross sections of Corriedale wool fibers. In order to differentiate A-cortex from B-cortex for each cross section, a photomicrograph of stained cross sections was supplemented (Fig. 14, a). The light absorption was measured with the unstained specimen sectioned in

succession to the former specimen. As can be seen in Fig. 14, b, the wool fibers are almost transparent against the visible light, but show a considerable absorption even in the region of near ultraviolet. Fig. 14, c shows the photomicrograph of cross sections of the wool taken with ultraviolet light having the wavelength of 313 mμ. At this wavelength A-cortex is less transmissible than B-cortex. The relation is reversed in the region of shorter wavelength than 280 mμ. Fig. 14, d shows the ultraviolet photomicrograph taken with the light having the wavelength of 265 mμ, in which one can see that A-cortex is more transmissible than B-cortex.

In order to authenticate the result of photomicrographic observations, the direct photometric measurements of absorption in the ultraviolet region were performed with a longitudinal section of a Lincoln wool fiber. A-cortex and B-cortex were subjected to the measurements separately. Fig. 15 shows the result. As can be seen in the figure, the optical density curves of A-cortex and B-cortex cross at the wavelength of about 290 mμ. In the region above 290 mμ A-cortex shows stronger absorption, while in the region below 290 mμ B-cortex shows stronger absorption.

The absorption in the region of longer ultraviolet is assumed to be due mainly to arginine and tryptophane residues which have strongly basic groups. The photometric result that A-cortex

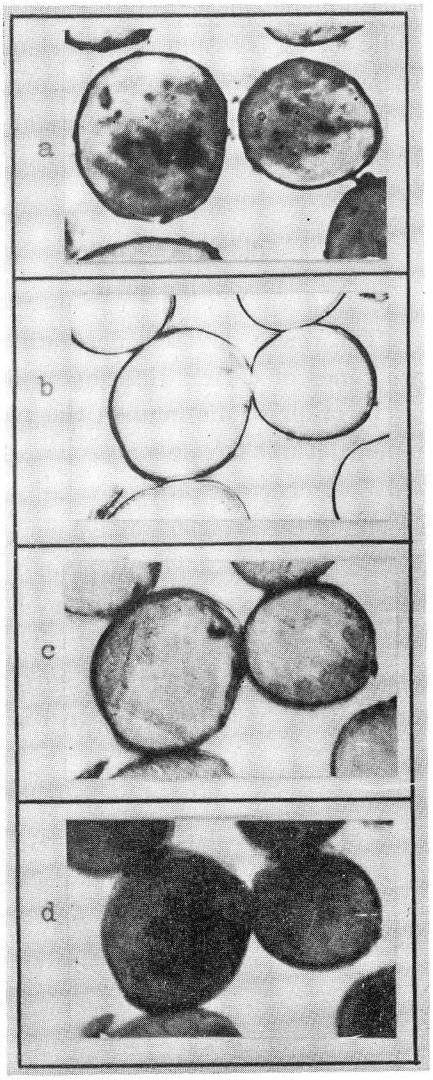

Fig. 14. Ultraviolet absorption of cross sections of wool fibers of Corriedale. (a) Stained by Methylene Blue and observed with visible light. B-cortex is stained in darker tone. (b) Not stained. Observed with visible light λ= 546 mμ. Entirely transmissible. (c) Not stained. Observed with ultraviolet light λ= 313mμ. A-cortex is less transmissible. (d) Not stained. Observed with ultraviolet light λ=265 mμ. B-cortex is less transmissible.

has a greater absorption at this region is consistent with the fact that A-cortex is relatively acidophilic.

The optical density curves of both the cortices have a prominent peak at about 280 mμ, which manifests the characteristic feature of tyrosine band, as was pointed out by Bendit[11] by the experiments with horse hairs. Since the absorption at this wavelength and in its neighborhood is the superposition of absorptions of several amino acid residues, it would not be appropriate beyond dispute to draw a conclusion, but an easiest assumption would be that B-cortex may be richer in tyrosine.

The absorption in the region below 260 mμ is too much complicated to be analysed, since almost all the amino acid residues existing in wool have their absorption in this region.

The mechanism of formation of bilateral structure could be elucidated in the case of rayon staple fibers, but this is beyond the reach of our knowledge in the case of wool fibers, at least under the present state. To unveil the secret extensive studies are

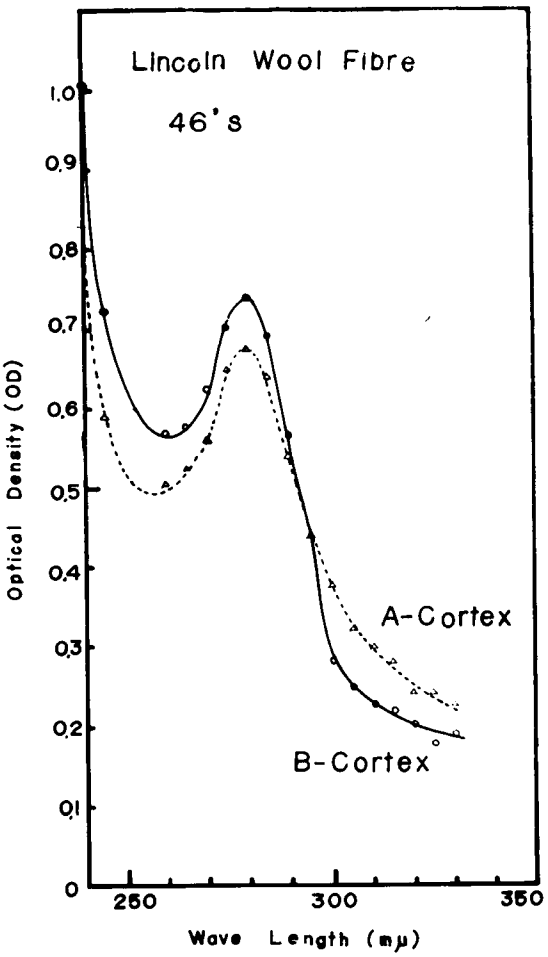

Fig. 15. Spectrophotometer curves of A-cortex and B-cortex of a Lincoln wool fiber.

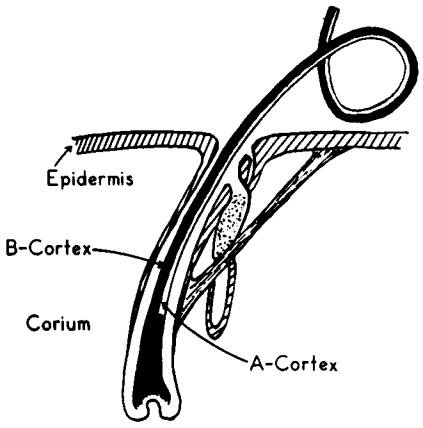

Fig. 16. Schematic representation of generating bilateral structure of a wool fiber in the skin.

required in the fields of biology and histology. But it is very interesting to note that the wool fiber is not bilateral at the vicinity of follicle, and has the staining property similar to the B-cortex. The A-cortex begins to appear at a point about one third the length of fiber from the root to the surface of skin, as schematically demonstrated in Fig. 16. This could be ascertained by slicing the skin of sheep in about 250 successive slices, each having the thickness of 5μ, and by observing the sections of fibers in each slice under a microscope. The slices had been stained by Methylene Blue to distinguish both the types of cortex.

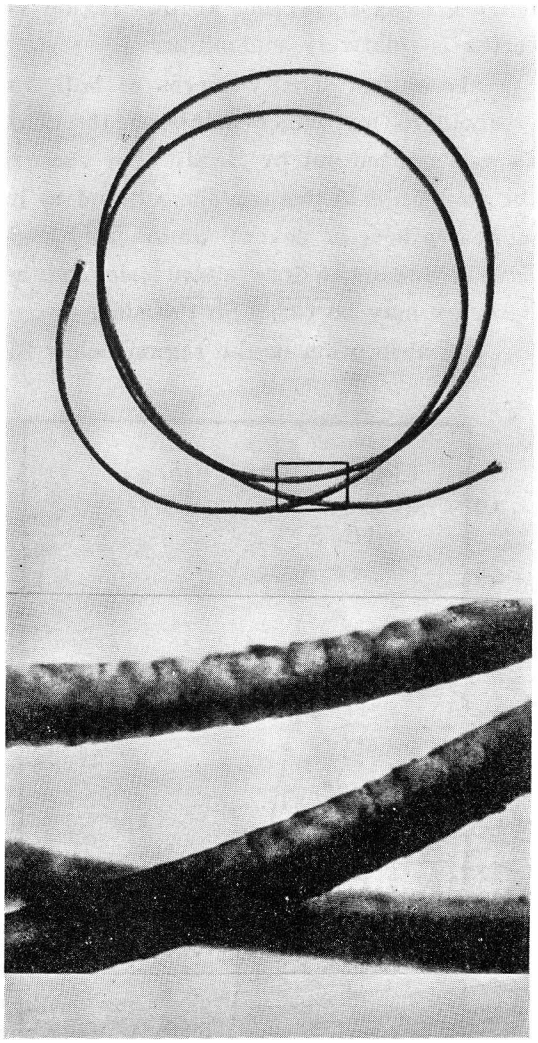

Fig. 17. Loops of a wool fiber stained by Janus Green. The outside of curvature is stained in darker tone as shown magnified in the lower photograph.

On account of the bilateral structure wool fibers have the intrinsic nature to coil. Thus, the fiber which was carefully straightened by steaming makes a coil on dipping in water. Fig. 17 shows the loops made in this manner, in which A-cortex is facing towards the inside of curvature. If individual fibers are separated, they tend to coil in their proper directions. This we can observe actually with the foetus of sheep, which has thin hair. Also in the matured sheep hairs grow in this manner on the shaved skin, as long as the hairs are very short. But, in general, the hairs of sheep grow close together and stick to each other during the growth by the action of scaly surface, grease and so forth, and form themselves into clusters of adhered hairs all over the skin. Therefore, the

individual fibers cannot act independently. Then, the theory developed with respect to the chips of crimped rayon staple applies to this case also, and the mechanical analysis of this system indicates that the individual fibers are apt to be twisted. This effect propagates itself all over the system, and eventually all the fibers in a lock tend to be in the same direction, and the wave is produced, each fiber being twisted by 180° at every transition from crest to trough, and *vice versa*. Fig. 18 shows the cross section of a waved lock, in which one can see that the fibers are facing in the same direction with respect to the bilateral structure, A-cortex pointing in the direction of bending. This figure is to be compared with Fig. 7 of the crimped rayon staple.

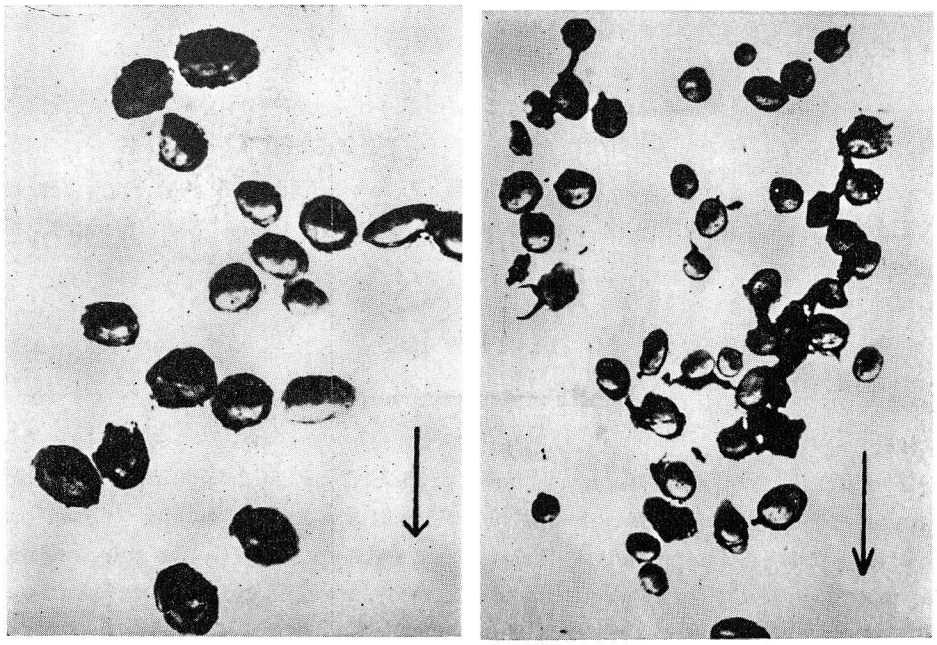

Fig. 18. Regular orientation of cross sections of fibers in a lock of wool. Stained by Janus Green. Arrow shows the direction of bending. A-cortex which is light in color points in the direction of bending. Compare this with Fig. 7 of crimped rayon staple.

Due to the difference in sensitivity of A-cortex and B-cortex to the medium, the curvature and the direction of bending change in manifold manners, depending upon the character of surrounding medium. This also has practical importance.

The microscopic observations reveal that A-cortex and B-cortex do not diffuse into each other, and a considerably sharp demarkation line can be postulated between them. Notwithstanding, it is very diffucult to separate

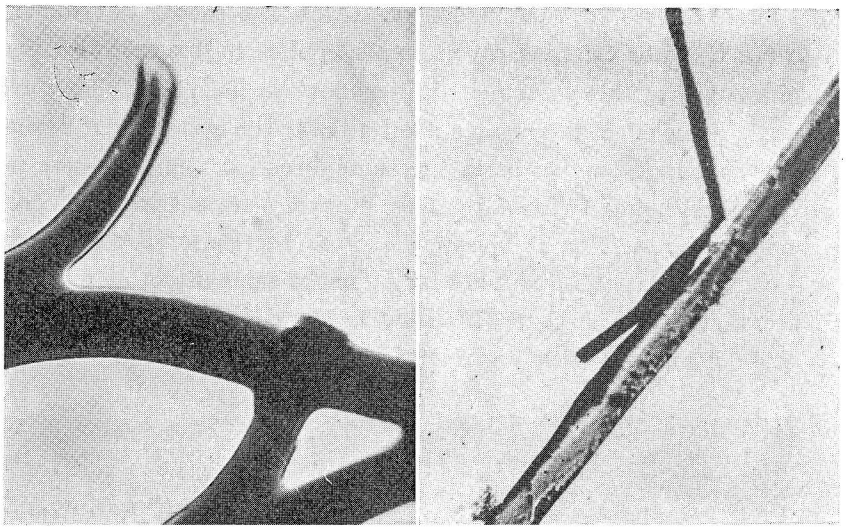

Fig. 19. Separation of A- and B-cortices by pyrolysis.

both the cortices from each other. Recently, we could find that they can be separated at the pyrolysis of wool fibers in a sealed tube. Fig. 16 shows an example.

SECTION III

Mechanics of Crimp

(a) Zig-zag spring

The man-made fibers such as those produced by melt spinning and dry spinning are generally straight in nature and have little crimp. Therefore, the crimp must be imparted to these fibers subsequently to the spinning and cold drawing, and this is done in practice by mechanical devices combined with thermosetting effect. One of the mechanical devices consists of pairs of finely pitched gears with sharply edged teeth. A tow of filaments is supplied between the pairs of gears, and teeth-marks are thermoset.

Another type of crimper which is used widely in textile industry consists of a thermosetting box provided with an inlet on one side and an outlet on the opposite side. A tape-like tow is compressed into the box through the inlet and folded many times over in a small pitch in the box and comes out of the outlet after the crimp is thermoset. The fibers crimped by these methods have on the whole a zig-zag shape. Fig. 20 shows a photomicrograph of the zig-zag fibers produced in this way on the commercial scale.

The dynamics of the plane zig-zag is relatively simple. The relation

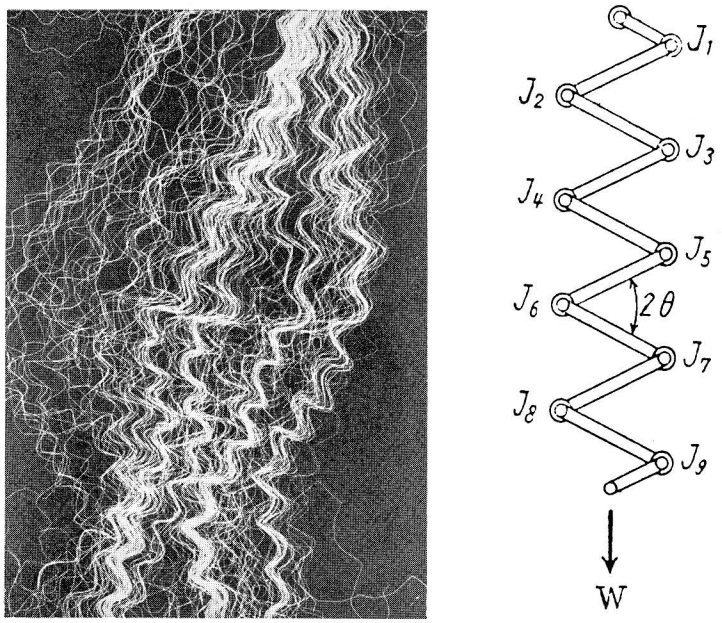

Fig. 20. Model of plane zig-zag, and photomicrograph of zig-zag-shaped staple.

between the angle between the adjacent zig-zag elements and the load can be expressed by

$$W = \frac{1}{k\left(\frac{l_m}{2n}\right)} \cdot \frac{\theta - \theta_0}{\cos\theta} \qquad (1),$$

where W is the load, θ_0 half of the initial angle between the elements, θ half of the angle between the elements after loading, n the number of the elements, l_m the length when the zig-zag is fully extended, and k a constant.

The constant k is determined by $d\theta/dM$, M being the moment of force acting upon the elements, and is assumed to be proportional to the reciprocal of EI_z, E being the modulus of elasticity, and I_z the moment of inertia of bending. Eq. (1) expresses that the load necessary to effect a certain degree of deformation of spring is proportional to the number of elements per extended length of spring on the one hand, and to EI_z on the other hand.

The spring constant K of zig-zag spring is given by

$$K = k\left(\frac{l_m}{2n}\right) = \frac{\theta - \theta_0}{\cos\theta} \Big/ W \qquad (2).$$

The experiments made with an ideal zig-zag spring made of a steel wire showed that the right-hand expression of Eq. (2) is constant, being consistent

with the relation given by Eqs. (1) and (2). Table 1 shows the result of the experiment.

Experiments were done also with the samples of zig-zag-shaped acetate staple, and the spring constant K was calculated by Eq. (2). The results are given in Table 2.

Table 1. Relation between load and deformation of a zig-zag spring made of a steel wire, and calculation of spring constant by Eq. (2).

Weight W (g)	Length of spring (mm)	Angle between elements (radian)	$\frac{\theta-\theta_0}{\cos\theta} \Big/ W = K$ (g^{-1})
0	19.8	0.7318	—
1	22.3	0.8430	0.168
3	25.2	1.0058	0.171
5	26.7	1.1088	0.157
7	27.6	1.1834	0.172
9	28.1	1.2302	0.167
11	28.5	1.2733	0.168
13	28.7	1.2960	0.165
15	28.8	1.3235	0.172
17	29.0	1.3454	0.165
19	29.1	1.3614	0.166
20	29.25	1.3780	0.168
50	29.7	1.4884	0.169
100	29.8	1.5708	—
			Average 0.167

Table 2. The load necessary to extend the zig-zag crimp of acetate staple and the calculation of spring constant by Eq. (2).

Sample A 5.4 den l_0 =20.2 mm l_m=23.4 mm			Sample B 5.0 den l_0 =22.6 mm l_m=25.0 mm			Sample C 3.7 den l_0 =21.7 mm l_m=25.9 mm		
Weight (mg)	Length (mm)	K (mg^{-1})	Weight (mg)	Length (mm)	K (mg^{-1})	Weight (mg)	Length (mm)	K (mg^{-1})
0	20.2	—	0	22.6	—	0	21.7	—
10	21.5	0.0032	10	23.7	0.037	10	24.0	0.050
20	22.3	0.036	20	24.1	0.032	20	24.7	0.041
30	22.7	0.039	30	24.4	0.034	30	25.0	0.040
40	23.0	0.046	40	24.6	0.038	40	25.3	0.040
50	23.1	0.046	50	24.7	0.037	50	25.4	0.039
100	23.4	—	80	24.9	0.048	100	25.7	0.035
			100	25.0	—	150	25.9	—
Average 0.040			Average 0.038			Average 0.040		

(b) Helical spring

In the case of the zig-zag spring the external stress is concentrated upon the junction points of the elements, and only the bending force responds to the external load. In the case of the helical spring, however, all the portions of the spring are responsible for the deformation caused by the external force, and both the bending and twisting forces of the spring material respond to the external stress. Therefore, the helical spring shows in general a greater resistance against the deformation due to the external force, so far as the spring consists of the same material and n/l_m is the same. The wool fibers in the fleece as it was sheared form planar waves, but in the course of individual operations the waves are so strongly deformed that most of the crimps have the shape of spiral coil, due to the intrinsic nature of wool fibers. The excellent property of wool crimp owes greatly to this shape factor. In the case of man-made fibers also it is desirable from the practical point of view to make the crimp having the shape of the helical spring.

As to the theoretical relation between the load and elongation of the helical spring which is so familiar to us there has been thus far but few publications in spite of its practical importance. Kondo[12] in our laboratory has elaborated to deduce the relation in the case when both the ends of a helical spring are prohibited from rotation. The relation is expressed as follows:

$$W = \frac{1}{\left(\frac{l_m}{2\pi n}\right)^2 \frac{m}{EI_z}\cos\theta} \cdot \left[\frac{m+1}{2}(\theta-\theta_0)+\frac{m-1}{2}(\sin\theta_0\cos\theta_0-\sin\theta\cos\theta)\right] \qquad (3),$$

and

$$EI_z = mGI_p,$$

where G is the rigidity and I_p the moment of inertia of twisting.

The value of the second term in the brackets of Eq. (3) is in general so small as to be neglected compared with that of the first term under the condition of measurement. Then the Eq. (3) is reduced to an approximate formula given by

$$W = \frac{1}{\frac{2}{m+1}\left(\frac{l_m}{2\pi n}\right)^2 \frac{m}{EI_z}} \cdot \frac{\theta-\theta_0}{\cos\theta} \qquad (4)$$

or

$$W = \frac{1}{\frac{2}{m+1}\left(\frac{l_m}{2\pi n}\right)^2 \frac{1}{GI_p}} \cdot \frac{\theta-\theta_0}{\cos\theta} \qquad (4').$$

The spring constant K is expressed by

$$K = \frac{2}{m+1}\left(\frac{l_m}{2\pi n}\right)^2 \frac{m}{EI_z} \qquad (5),$$

or $$K = \frac{2}{m+1}\left(\frac{l_m}{2\pi n}\right)^2 \frac{1}{GI_p} \qquad (5').$$

The load W is proportional to EI_z, as was the case with zig-zag spring, but a conspicuous difference consists in the fact that load W is proportional to the square of the number of turns per extended length of spring contrary to the case of zig-zag spring, where the load is proportional simply to the number of elements per extended length.

The applicability of Eqs. (4) and (5) was examined by a model spring made of steel wire having a circular cross section. Table 3 shows the result.

Table 3. Relation between the load and deformation of helical spring made of steel wire and calculation of spring constant.

$d=0.502$ mm $l_m=1925$ mm $n=3\frac{1}{2}$

Weight (g)	Length of spring (mm)	Tilting angle of spiral (radian)	Spring constant K (g^{-1})
0	240	0.1248	—
3.9	400	0.2092	0.0221
7.0	500	0.2627	0.0204
10.3	600	0.3171	0.0196
13.7	700	0.3721	0.0194
17.5	800	0.4285	0.0191
21.5	900	0.4864	0.0190
22.6	1,000	0.5463	0.0193
31.2	1,100	0.6082	0.0189
37.7	1,200	0.6731	0.0186
43.7	1,300	0.7415	0.0191
52.4	1,400	0.8145	0.0192
67.1	1,500	0.8933	0.0183
85.0	1,600	0.9812	0.0181
110.4	1,700	1.0824	0.0185
			Average 0.0193

The value of K calculated from Eq. (5) putting $E=2.1\cdot10^7\ \mathrm{g\cdot mm^{-2}}$ and $m=1.25$, which are the values of the steel, is $0.0192\ \mathrm{g^{-1}}$ and agrees quite exactly with the observed value.

The similar experiments were done with a series of samples of bilateral fibers with helical crimps. As an example, the result obtained with a bilateral nylon fiber consisting of nylon 66 and nylon 6 is given in Table 4. The fiber has helical crimps, as shown in Fig. 42. In this case the value of m would differ considerably from unity, but the values of K calculated by Eq. (5) are almost constant, and this verifies that Eq. (4) applies to the practical textile

Table 4. Relation between the load and deformation of bilateral helical fibers consisting of nylon 66 and nylon 6, and calculation of spring constant.

$d=0.0673$ mm $l_m=46.5$ mm $n=9\frac{1}{4}$

Weight (mg)	Length of helical fiber (mm)	Tilting angle of helix (radian)	Spring constant (mg^{-1})
0	29.0	0.6734	—
9.1	30.0	0.7000	0.00382
19.8	31.0	0.7296	0.00381
31.7	32.0	0.7589	0.00372
45.0	33.0	0.7889	0.00364
56.7	34.0	0.8200	0.00387
70.0	35.0	0.8520	0.00387
86.7	36.0	0.8855	0.00387
111.0	37.0	0.9201	0.00367
133.3	38.0	0.9565	0.00369
166.7	39.0	0.9948	0.00354
198.3	40.0	1.0375	0.00358
230.0	41.0	1.0795	0.00374
281.0	42.0	1.1272	0.00376
360.0	43.0	1.1793	0.00369
496.7	44.0	1.2416	0.00376
716.7	45.0	1.3163	0.00356
			Average 0.00372

fibers spun by the conjugate spinning method.

The spring constant K was calculated by using the observed value of the modulus of the fiber $E=2.5\cdot10^{10}$ dynes/cm^2. It is expected that the value of m would be from 5 to 7. For the calculation m was assumed to be 6. The calculated value of K is 0.00381 and very close to the observed value.

As can be deduced from the theory, the load necessary to effect a certain degree of deformation of zig-zag spring is proportional to the number of elements per unit length of the extended spring, that is — proportional to n/l_m, while in the case of the helical spring the load is proportional to the square of number of turns per extended length of spring, that is — proportional to $(n/l_m)^2$. This is verified by the experiments with the zig-zag spring and helical springs made of steel wire, as shown in Fig. 21.

The helical spring exerts always the greater resistance to the external force than the zig-zag spring. As shown above, the mechanical response of the helical spring is intensely influenced by the shape factor, and a fine pitched helical spring is the most desirable shape of textile fibers to exert a

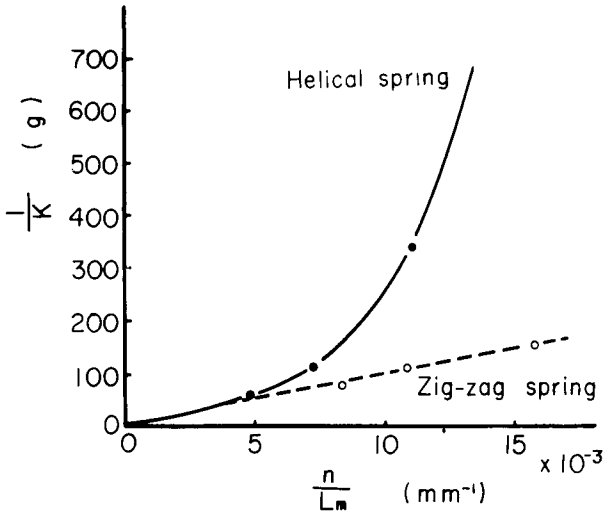

Fig. 21. Reciprocal of spring constant as a function of n/l_m for zig-zag spring and helical spring.

wooly effect.

SECTION IV

Production of Helical Fibers by Melt Spinning

Our theory of crimp under consideration of bilateral structure has been realized also in the field of fully synthetic fibers, as is represented by the commercial production of bicomponent acrylic fibers, Orlon Sayelle of Du Pont Company. According to Hicks et al.[13], the fiber is bilaterally structured and is provided with the inherent nature of producing three dimensional reversible crimp as a result of its response to heat and moisture.

A project of producing bilateral fibers by melt spinning has been undertaken for the past several years by us. Besides the side-by-side conjugation of the two components along the fiber axis, as can be seen in the photomicrograph of cross sections in Fig. 22, a new type of conjugation fiber was made, in which the second component is eccentrically enclosed in the first component, as shown in Fig. 23. The latter type would be useful for the pair of components which are not stably bound to each other, and are apt to be separated by mechanical treatments.

Most of the composite fibers produced by melt spinning have little crimp as they were spun and stretched, but produce fine crimp spontaneously on heating them up to a temperature higher than that of stretching. Fig. 24

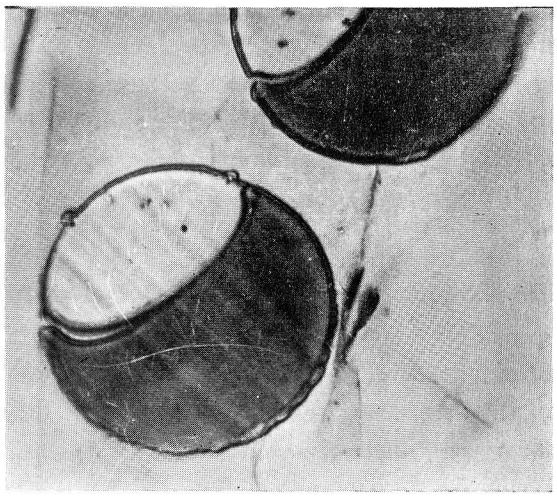

Fig. 22. Cross sections of bilaterally conjugated fibers made of nylon 6 (stained) and polyethylene terephthalate.

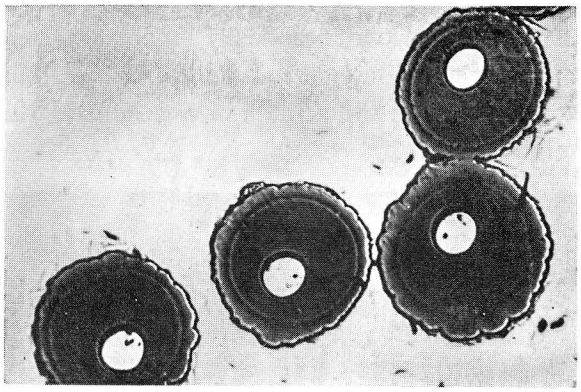

Fig. 23. Cross sections of eccentrically conjugated fibers made of nylon 6 (stained and enveloping) and polyethylene terephthalate (unstained and enclosed).

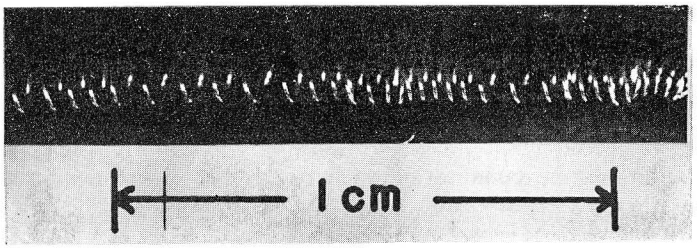

Fig. 24. Helical spring of two component filacement made of nylon 6 and polyethylene terephthalate. The cross sections are similar to those shown in Fig. 22.

shows the helical coil of the two-component fiber, whose pitch of spiral is as fine as to be comparable with the diameter the fiber.

A series of our researches on this line authenticates that helical fibers can be produced by the process of melt spinning which is modified so as to furnish the fibers with bilateral structure or eccentric structure.

SECTION V

Oriented Overgrowth of Crystalline Polymers–Epitaxy

The experiments of conjugate melt spinning have been done with a number of polymer pairs of practical interest. In some pairs the union of components was so strong that they were not separated from each other in a sequence of processings such as spinning, stretching, heat treatment, repeated stretching and releasing, rubbing, beating and so forth. In some other polymer pairs, however, the cohesion between the components was relatively weak, and they were disjoined at a certain stage of processing. Fig. 25 shows a photomicrograph of conjugate-spun fiber made from high density polyethylene and isotactic polypropylene. These two practically important polyolefins make a very excellent conjugate fiber having fine helical crimps, but they are very readily separated by repeating the stretch or even during the time of leaving it still at room temperature.

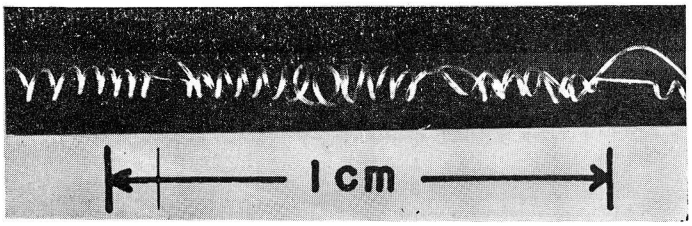

Fig. 25. Conjugate spun fiber made from polyethylene and polypropylene. Disjoined at places.

This induced us to direct our attension to the compatibility of the two polymers. The strongest force between the polymer molecules would be the crystalline force. As a matter of fact, there is a possibility that the two components have a share in the same crystalline domain, as will be treated in the next chapter.

Another point to be considered with respect to the cohesion would be the condition of the boundary surface between the two elements. One of the interfacial phenomena between the two crystalline substance is the oriented overgrowth or epitaxy. This can happen when the one-dimensional or two-

dimensional structure analogy between both the crystals is found, although it also seems to be necessary that the congruent plane of molecules exists. The foundation for the structural study on the epitaxy was laid down a long time ago, but it is only recently that the oriented overgrowth of polymer substances has been discussed from the crystallochemical standpoint of view.

Willems[14] has found the oriented overgrowth of polyethylene on the clean face of rock salt, and later Eppe et al.[15] and Fischer[16] have shown that the polyethylene is oriented with its (110) plane parallel to the (001) plane of substrate, and with its molecular chains parallel to the [110] direction of the sodium chloride.

The paraffin wax-polyethylene system is the ideal for the occurrence of oriented overgrowth, as pointed out by Richards[17]; in each case the C–C bonds of molecules form a plane zig-zag, and the crystal structures of both the substances are very closely similar. The evaluation of the oriented overgrowth of paraffin wax crystals on the spherulites of polyethylene by Willems[18] and on the surface of drawn film of polyethylene by Richards[17] reveals that the molecules of paraffin wax are oriented in parallel to the polyethylene molecules. Fig. 26 shows the oriented overgrowth of paraffin wax crystals on the surface of the drawn film of polyethylene taken by us.

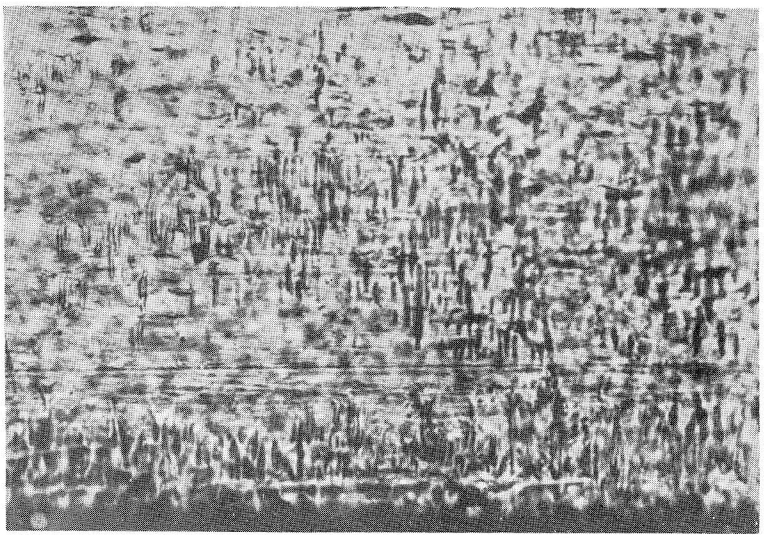

Fig. 26. Oriented overgrowth of paraffin wax crystals on the surface of drawn sheet of polyethylene. Paraffin wax crystals deposit standing on the edge so that c-axis points in the direction of drawing, which is horizontal in this figure.

Although the backbone of isotactic polypropylene also consists of C–C bonds, it is not a plane zig-zag, contrary to the case of paraffin wax and polyethylene, but is helical and has the three-fold screw symmetry. Therefore, in spite of the very close chemical resembrance of polyethylene and polypropylene, the congruent plane is not realized for both the crystals. This applies to the system of paraffin wax and polypropylene. Fig. 27 shows the growth of paraffin wax crystals on the surface of the drawn film of polypropylene. Contrary to the oriented overgrowth of paraffin wax on polyethylene (Fig. 26), there takes place no regular orientation of crystal growth of paraffin wax on isotactic polypropylene. This suggests also that the oriented overgrowth of polyethylene on polypropylene and *vice versa* would not happen, and the interfacial cohesion of both the crystals will not be strong enough.

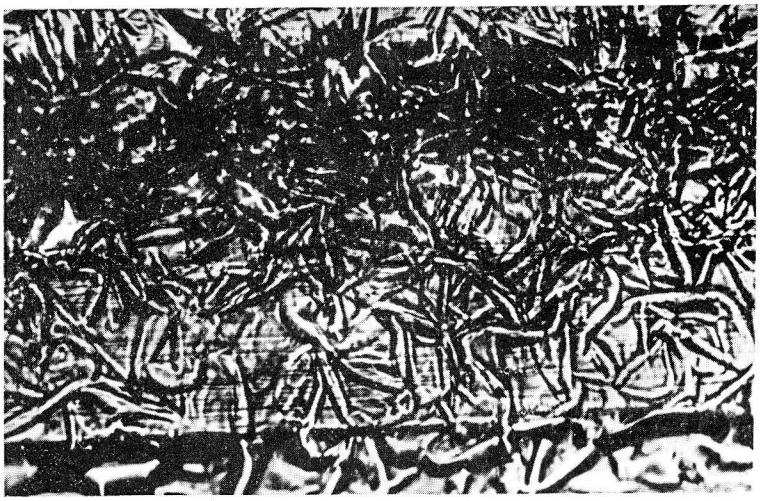

Fig. 27. Random growth of paraffin wax crystals on the surface of drawn sheet of polypropylene. The direction of drawing is horizontal in this figure. The boundary line at the bottom of the figure is that between a drawn polyethylene sheet and a glass sheet.

Although the epitaxy is at present not uniquely useful for a criterion to determine the affinity of the two crystalline polymers, the result obtained with polyethylene and polypropylene is consistent with the result of spinning experiments which showed the lack in stability of the conjugate fibers made from both the polyolefins, as already shown in Fig. 25.

Richards has shown that there is no oriented overgrowth of paraffin wax crystals on nylon 66 in spite of the existence of the very close one-dimensional analogy along the chain axis. This applies to the system of paraffin wax-nylon 6, as is actually shown in Fig. 28. Since paraffin wax and polyethylene are very closely similar, it is postulated that the oriented overgrowth would

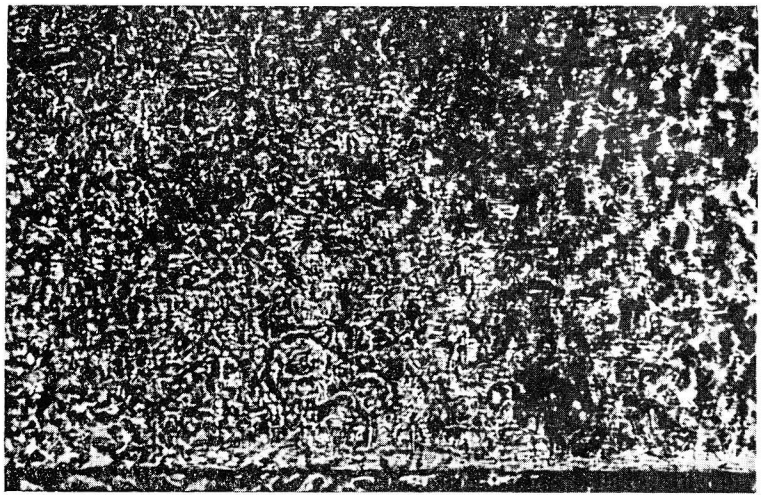

Fig. 28. Random growth of paraffin wax crystals on the surface of drawn sheet of nylon 6. The direction of drawing is horizontal in this figure. The boundary line at the bottom of the figure is that between a drawn sheet of nylon 6 and a glass sheet.

not take place in the system of polyethylene-nylon 6. Similar conclusion is obtained with respect to the system of polypropylene-nylon 6. The results of the conjugate spinning are consistent with the assumption; the bilateral fibers consisting of polyethylene and nylon 6, or polypropylene and nylon 6

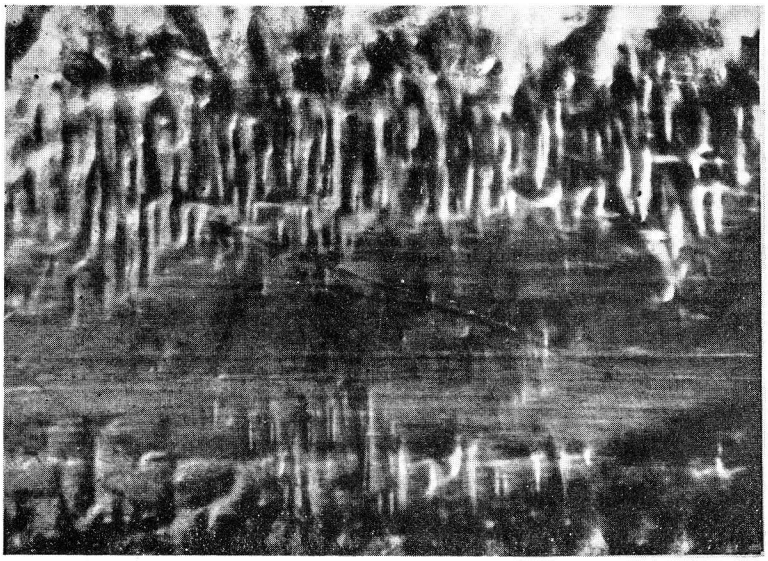

Fig. 29. Oriented overgrowth of paraffin wax on the surface of drawn sheet of polyoxymethylene (Derlin). The direction of drawing is horizontal in this figure.

are readily separable.

So far as we know, there is no evidence of oriented overgrowth in polymer-polymer system. This we could find in the polyethylene-polyoxymethylene (Derlin) system. As can be seen in Fig. 29, the paraffin wax crystallizes on the drawn sheet of polyoxymethylene so that c-axis points to the molecular direction of polyoxymethylene, as is the case with the paraffin wax-polyethylene system (Fig. 26). Fig. 30, a shows the diffraction pattern of the drawn polyoxymethylene film with the x-ray beam perpendicular to the film surface, whilst Fig. 30, b shows the diffraction pattern of the same sheet with paraffin wax crystals grown on the surface. It is seen that the intensity of (110) and (200) reflection of paraffin crystal is greater around the equator, showing that the c-axis of paraffin crystals orients preferably in parallel to the c-axis of polyoxymethylene. The long arcs are due to the disturbed orientation at the upper layer of paraffin wax.

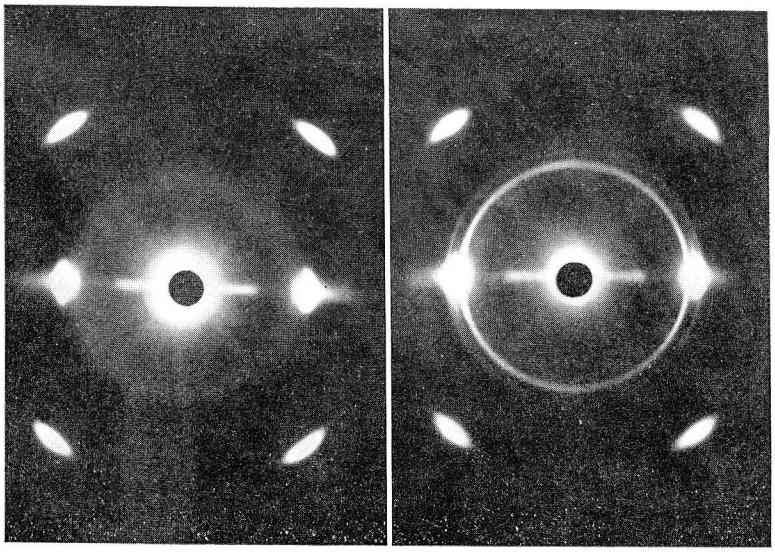

a b

Fig. 30. Diffraction pattern of drawn film of polyoxymethylene (a), and that of the film with paraffin wax overgrown on it (b). The pattern of paraffin wax shows the tendency of orientation of molecules.

Similar orientation is found with the polyethylene crystals overgrown on the cold drawn sheet of polyoxymethylene, as shown in Fig. 31. In this case also, the directions of c-axis of both the polymers are congruent. The two-dimensional similarity of both the crystals is demonstrated in Fig. 32. The repeating distance along the molecular axis of polyoxymethylene is 17.3A, which is near seven times the period of polyethylene, 17.7A, and the mismatch

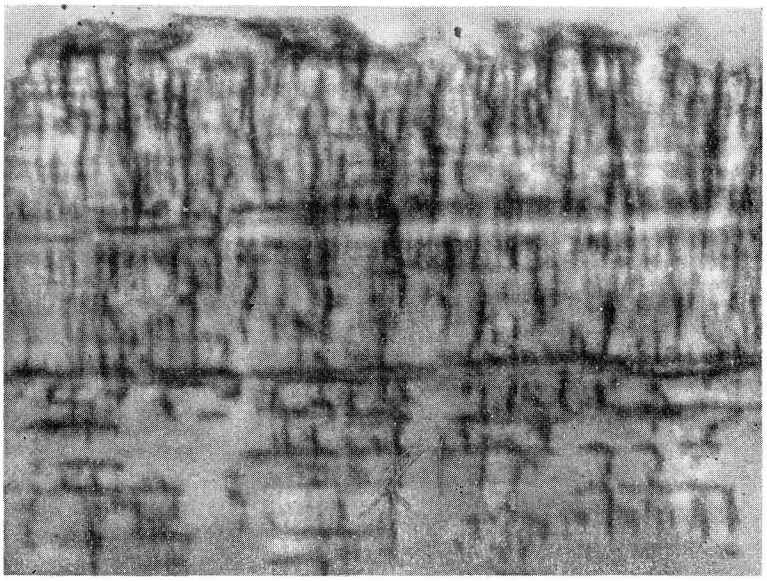

Fig. 31. Oriented overgrowth of polyethylene crystals on the drawn sheet of polyoxymethylene. The direction of drawing is horizontal in this figure.

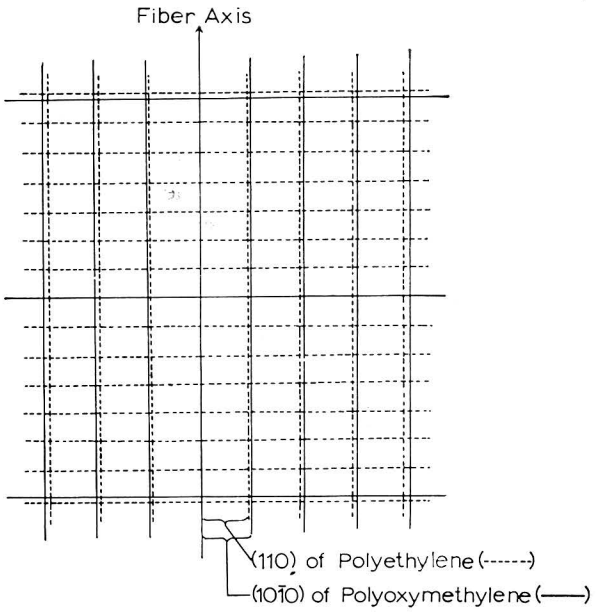

Fig. 32. The two-dimensional similarity of polyethylene and polyoxymethylene crystals.

is only 2.2%. The distance between the molecular chains is 4.46A for polyoxymethylene, and 4.43A for polyethylene, the mismatch being smaller than 1%. Therefore, there is a very close two-dimensional analogy between the two

crystals. There is, however, a conspicuous difference in the arrangement of atoms of chain elements; the backbone of polyethylene consists of a plane zig-zag, while that of polyoxymethylene is helical.

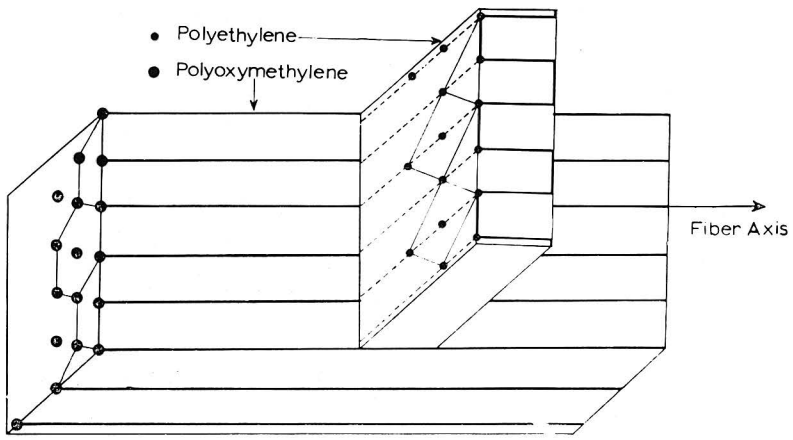

Fig. 33. Schematic representation of the manner of deposit of a polyethylene crystal upon the crystal of polyoxymethylene.

Fig. 33 is the three dimensional sketch of the oriented overgrowth of polyethylene upon the cold-drawn polyoxymethylene film; the crystal of polyethylene stands on edge with the (110) plane parallel to the surface of sheet. The molecule of polyethylene is folded within the (110) plane, with the c-axis parallel to the c-axis of polyoxymethylene. The height of overgrown crystals of polyethylene is estimated at 3000-5000A by the electron microscopic observations. The electron diffraction pattern of the overgrown crystals of polyethylene shows the distinct feature of fiber diagram, as shown in Fig. 34, and indicates that c-axis is parallel to the molecular direction of polyoxymethylene.

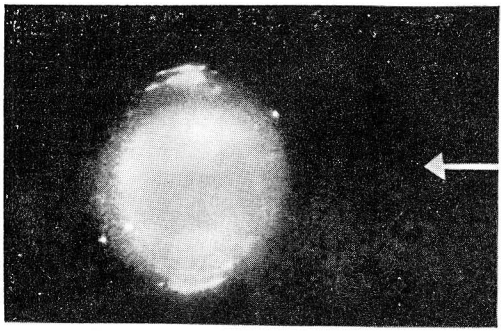

Fig. 34. Electron diffraction pattern of a polyethylene crystal grown on the surface of drawn film of polyoxymethylene. Arrow showes the direction of molecular chains (c-axis).

The oriented overgrowth of polyethylene crystals takes place also on the single crystals of polyoxymethylene. The regularly oriented layer of single crystals

of polyoxymethylene can be obtained by crystallizing it upon the (001) plane of rock salt, as shown in Fig. 35. Now, there are two possible manners of oriented overgrowth of polyethylene single crystals upon those of polyoxymethylene. One of these is demonstrated in Fig. 36. The angles between (110) plane of polyethylene and the crystal habit planes of polyoxymethylene are 3°41′, 56°19′ and 63°41′, respectively. This is realized, as can be seen in an electron photomicrograph of Fig. 37.

Another possible type of oriented overgrowth is demonstrated in Fig. 38, where the angles between the crystal habit planes of polyethylene and that of polyoxyme-

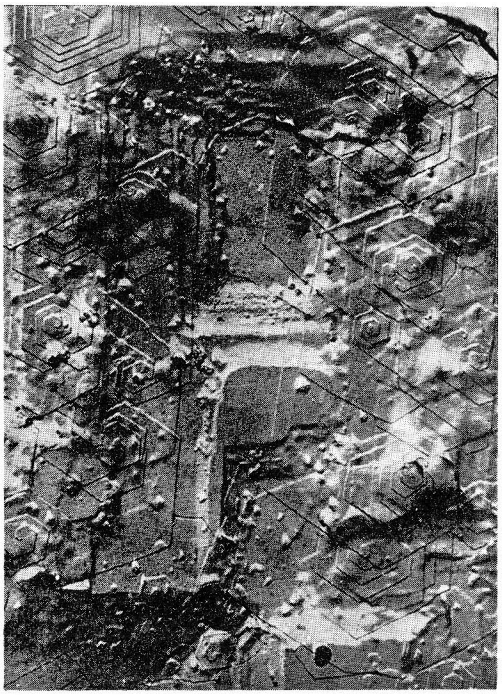

Fig. 35. Oriented overgrowth of polyoxymethylene crystals on the surface of rock salt.

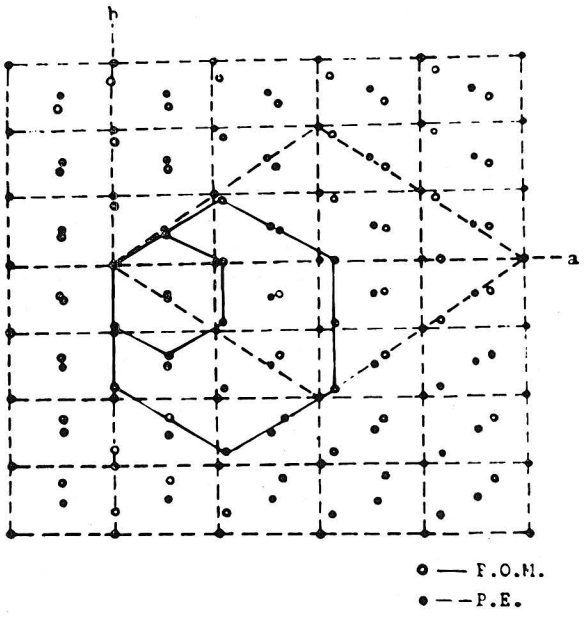

Fig. 36. A possible manner of oriented overgrowth of a polyethylene single crystal upon a single crystal of polyoxymethylene.

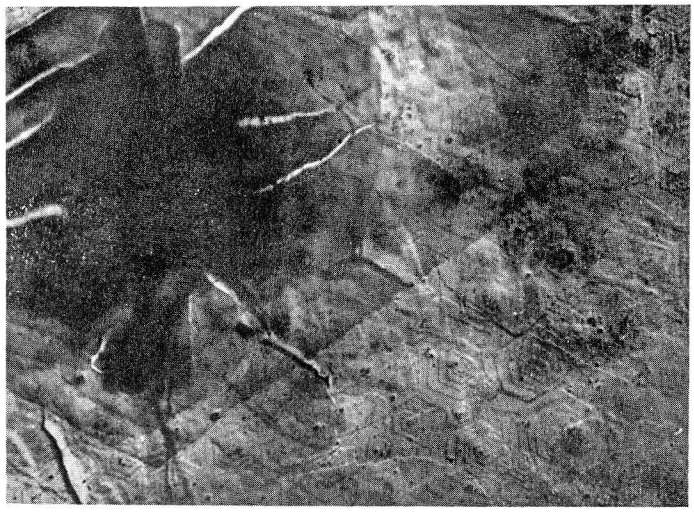

Fig. 37. Electron photomicrograph of oriented overgrowth of polyethylene single crystals upon those of polyoxymethylene. The manner of orientation agrees with that shown in Fig. 36.

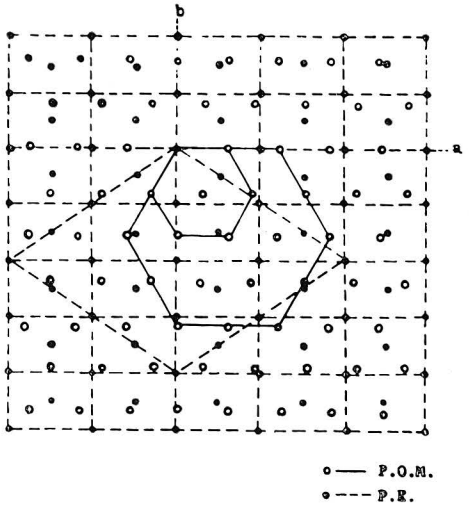

Fig. 38. Another possibility of oriented overgrowth of a polyethylene single crystal upon a single crystal of polyoxymethylene.

thylene are 26°19′, 33°41′ and 86°19′, respectively. The electron photomicrograph of Fig. 39 certifies this as correct.

The electron diffraction patterns of polyoxymethylene single crystals with polyethylene single crystals overgrown on them authenticate the existence of

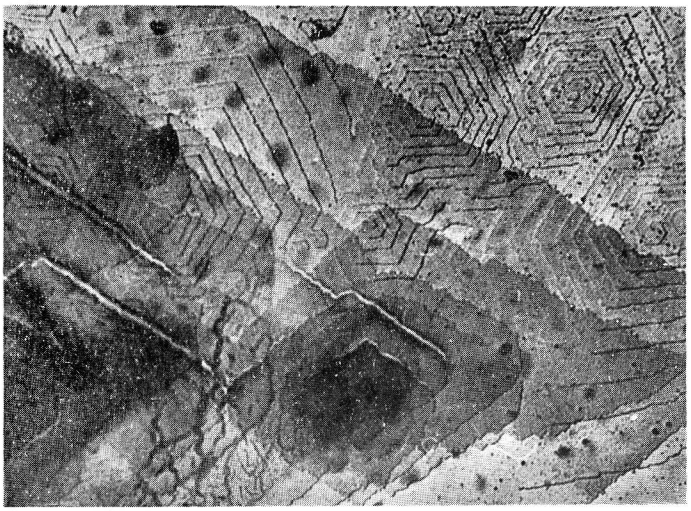

Fig. 39. Electron photomicrograph of oriented overgrowth of polyethylene single crystals upon those of polyoxymethylene. The manner of orientation agrees with that shown in Fig. 38.

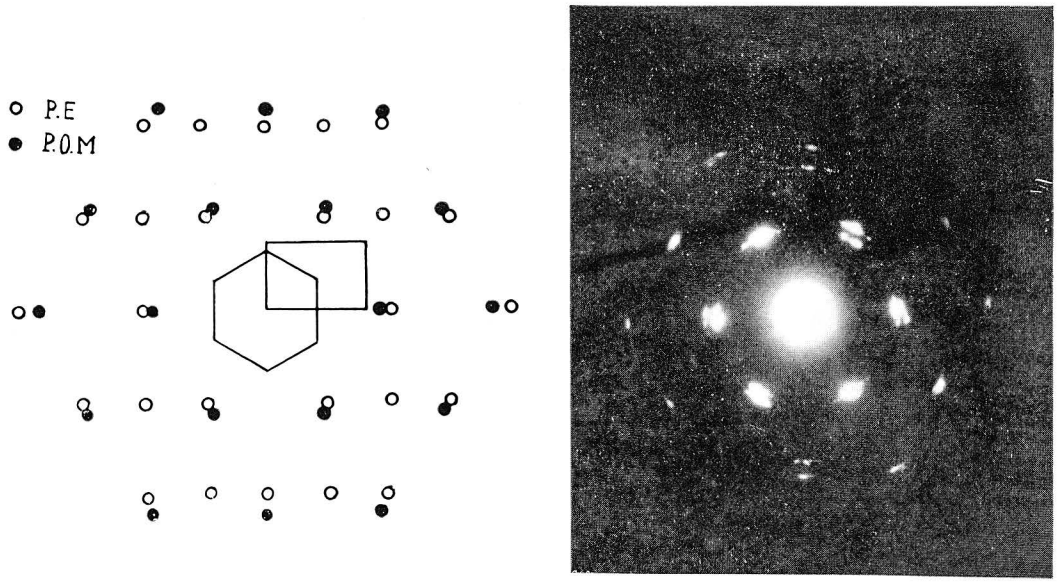

Fig. 40. Electron diffraction pattern of polyoxymethylene single crystal with a polyethylene single crystal overgrown in a manner shown in Figs. 36 and 37 in comparison with the reciprocal lattice points. Correspondence is almost perfect.

two types of oriented overgrowth, as shown in Figs. 40 and 41.

The oriented overgrowth of polymer-polymer system gives a number of

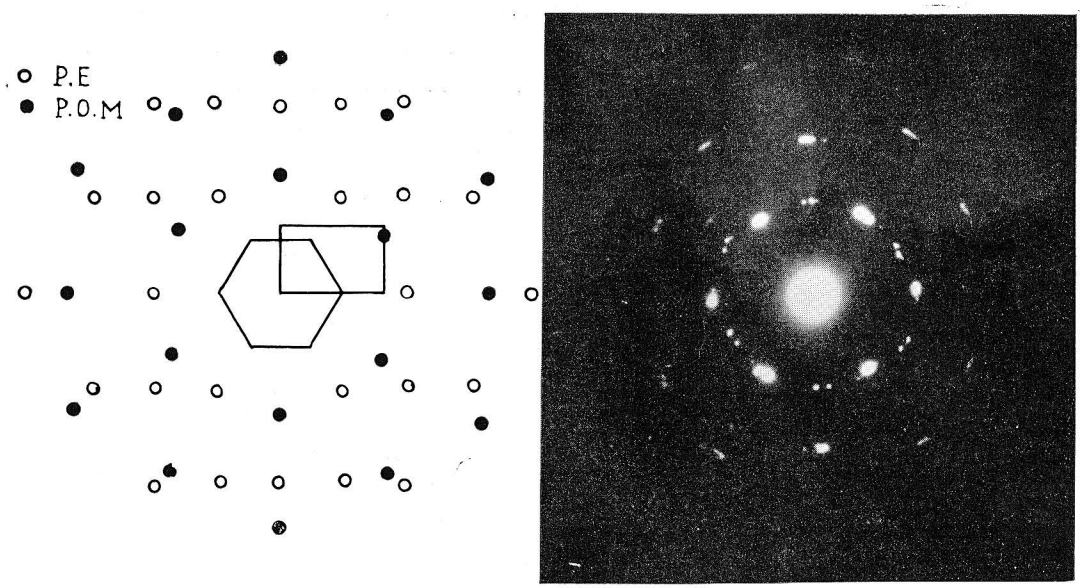

Fig. 41. Electron diffraction pattern of polyoxymethylene single crystal with a polyethylene single crystal overgrown in a manner shown in Figs. 38 and 39 in comparison with the reciprocal lattice points. Correspondence is almost perfect.

interesting suggestions bearing on the structure study on high polymers, and is also a subject of our research.

We have tried to make a fiber consisting of polyethylene and polyoxymethylene, but, thus far, we have not been able to obtain a sample of polyoxymethylene which is suitable for fiber spinning.

The epitaxy would be indeed one of the criterions to find the polymer pairs having strong affinity, but would not be a unique standard. According to Richards, paraffin wax crystals orient on the cold-drawn sheet of polyethylene sebacate. This suggests that the oriented over-growth of polyethylene crystals would take place on the surface of the drawn sheet of polyethylene sebacate. However, the bilateral fibers composed of these two polymers in various ratios proved to be readily separable, contrary to expectation.

SECTION VI

Chemical Analogy between Polymers

Epitaxy results from the dimensional structure analogy of crystals, regardless of the binding forces between substrate and deposit, which can comprise all kinds of primary valences, secondary valences, ionic forces, hydrogen

bonds and so forth. The epitaxy indeed serves as a measure of affinity of two crystalline polymers, as exemplified by the pair of polyethylene and polypropylene, which are closely relative to each other in the chemical sense, but have no dimensional analogy and are readily separable. However, we can find a number of polymers which are chemically relative to each other and have also the structural similarity to some extent. The affinity between these polymers is assumed to be greater than that resulting only from the dimensional analogy of crystals.

One of the good evidences is the system nylon 66-nylon 6, which are chemically closely allied and have very close dimensional similarity; the identity period is exactly the same, and the dimensions of basal plane also are very alike. These two polyamides have a strong affinity, and the bilaterally conjugated crimped filaments made of them are stable against the mechanical handlings. Fig. 42 shows the helical crimps and cross sections of bilateral nylon filaments consisting of nylon 66 and nylon 6.

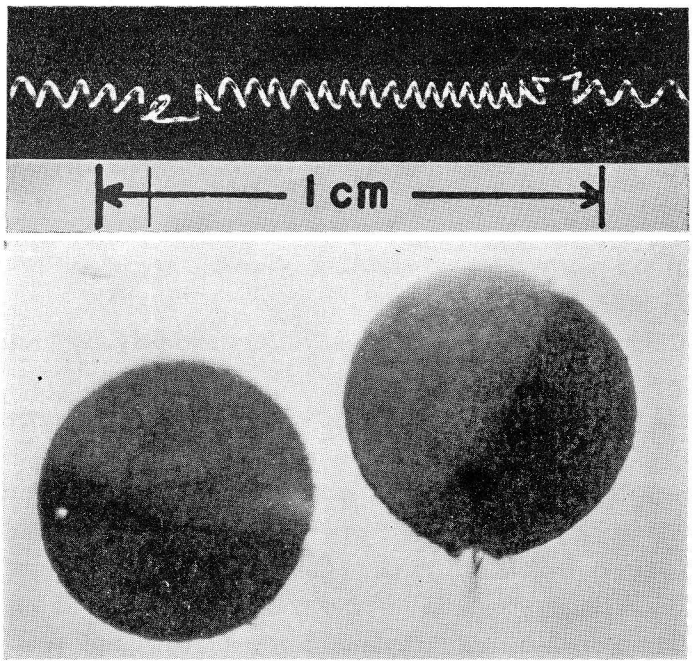

Fig. 42. Upper. Helical crimps of bilateral nylon filament consisting of nylon 66 and nylon 6.
Lower. Cross sections of nylon 66/nylon 6 conjugate fibers. Stained by Cibaron Violet which stains nylon 6 in darker tone than nylon 66.

To know the affinity between polymers, a series of experiments has been done with a number of co-polyesters and co-polyamides, and the melting points of bicomponent copolymers were measured as a function of composition.

The dibasic acids used for the preparation of polyesters and polyamides are as follows:

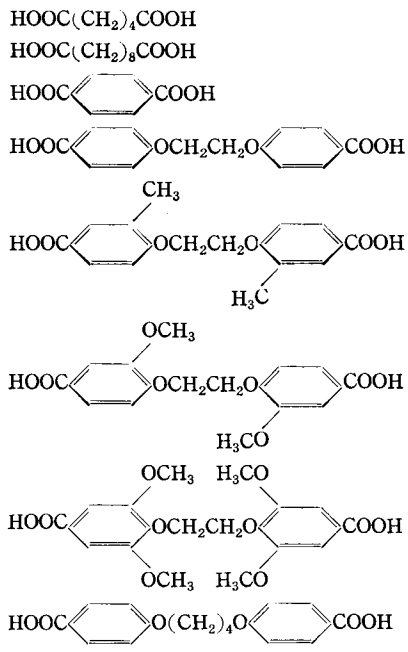

$HOOC(CH_2)_4COOH$ Adipic acid

$HOOC(CH_2)_8COOH$ Sebacic acid

Terephthalic acid

1, 2-bis (4-carboxyphenoxy) ethane, "B-ic acid"

1, 2-bis (2-methyl-4-carboxyphenoxy) ethane, "M-ic acid"

1, 2-bis (2-methoxy-4-carboxyphenoxy) etnane, "V-ic acid"

1, 2-bis (2, 6-dimethoxy-4-carboxyphenoxy) ethane, "S-ic acid"

1, 4-bis (4-carboxyphenoxy) butane, "Bu-ic acid"

As the glycol and diamine component, ethylene glycol and hexamethylene diamine were used.

The melting points of a series of polyesters and polyamides are tabulated in Table 5.

Edgar and Hill[19] measured as a function of composition the melting points of co-polyesters based on polyethylene terephthalate, which have ethylene adipate and ethylene sebacate as the second component, respectively, and referred to the theory presented by Flory[20]. The depression of melting points of the co-polyesters took place to the same degree with each of the second ingredients mentioned above up to the content of about 60 molar percent, and the heat of fusion per ethylene terephthalate unit was determined to be about 2200 calories, according to the theory of Flory. Similar experiments were performed with a series of co-polyesters based on polyethylene terephthalate which have as the second component, ethylene B-ate, M-ate, V-ate and Bu-ate, respectively. The results are shown in Fig. 43. It is very

Table 5. Melting points of polyesters and polyamides employed in experiments.

Polyesters		
Dibasic acids	Glycol	Melting point* (°C)
$HOOC(CH_2)_4COOH$	$HOCH_2CH_2OH$	47
$HOOC(CH_2)_8COOH$	"	72
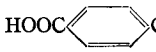	"	258
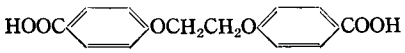	"	245
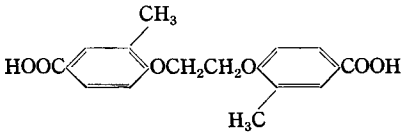	"	242
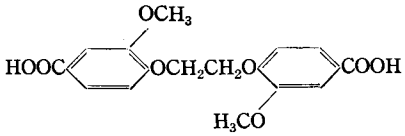	"	207
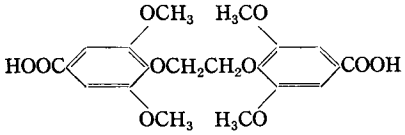	"	154
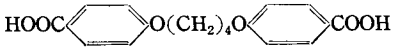	"	217
Polyamides		
Dibasic acid	Diamine	Melting point
$HOOC(CH_2)_4COOH$	$H_2N(CH_2)_6NH_2$	263
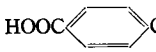	"	>300

* Measured by the hot-stage microscope method.

interesting to note that these ingredients also affect the depression of melting point almost to the same extent as ethylene adipate and ethylene sebacate studied by Edgar and Hill.

Experiments were done next with the copolymers based on polyethylene B-ate which have as the second component ethylene adipate, sebacate, terephthalate, B-ate, V-ate, M-ate and S-ate, respectively. The results are shown in Fig. 44. The dibasic acid ingredients except M-acid give rise to almost the same depression of melting point, and Flory's plots of $1/T_m$ vs. $-lnX$, T_m being the melting point of the co-polyester and X the molar fraction of the base component, result in the heat of fusion of ethylene B-ate unit of about

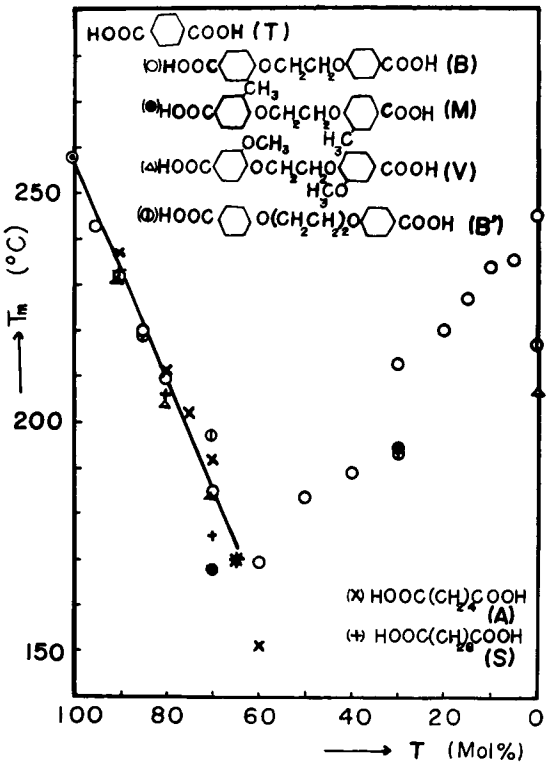

Fig. 43. Melting point vs. composition curves of co-polyesters based on polyethylene terephthalate with ethylene B-ate, M-ate, V-ate and Bu-ate as a second component, respectively. The data of co-polyesters with ethylene adipate and ethylene sebacate as a second component are supplemented.

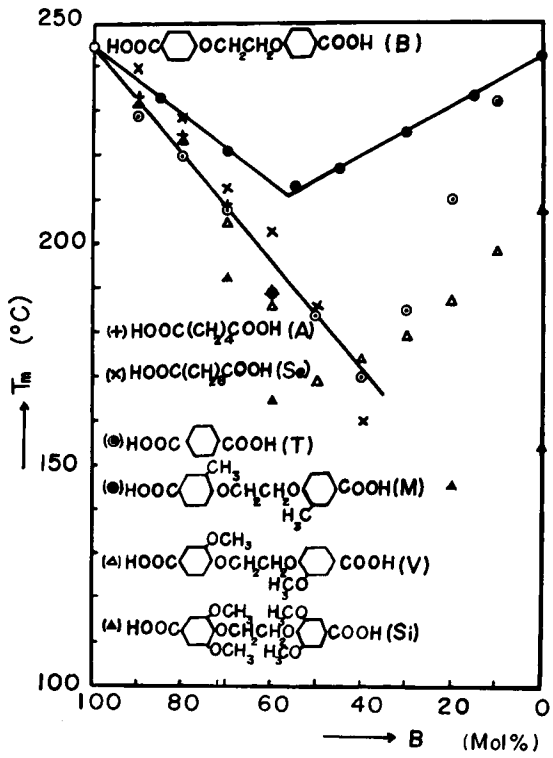

Fig. 44. Melting point vs. composition curves of co-polyesters based on polyethylene B-ate with ethylene adipate, sebacate, terephthalate, V-ate, M-ate and S-ate as a second component, respectively.

5000 calories. The depression is distinctly smaller for the co-polyester which has ethylene M-ate as the second component. This would mean that the crystallization of the base component of polyethylene B-ate is disturbed to a smaller extent by the M-ic acid ingredient, and suggests the mixed crystallization or formation of isomorphous mixtures as happening. B-ic acid and M-ic acid are most closely allied in chemical constitution; the difference is only that the latter has methyl groups at 2 and 2′ positioned carbon atoms in the phenylene groups.

The further examples are given in Figs. 45 and 46. Fig. 45 shows the melting points of the co-polyesters, that is —polyethylene M-ate/B-ate, polyethylene M-ate/V-ate and polyethylene M-ate/terephthalate. Ethylene B-ate and ethylene V-ate which have similar chemical constitution to the basic component of M-ate bring about smaller depressions than ethylene terephthalate.

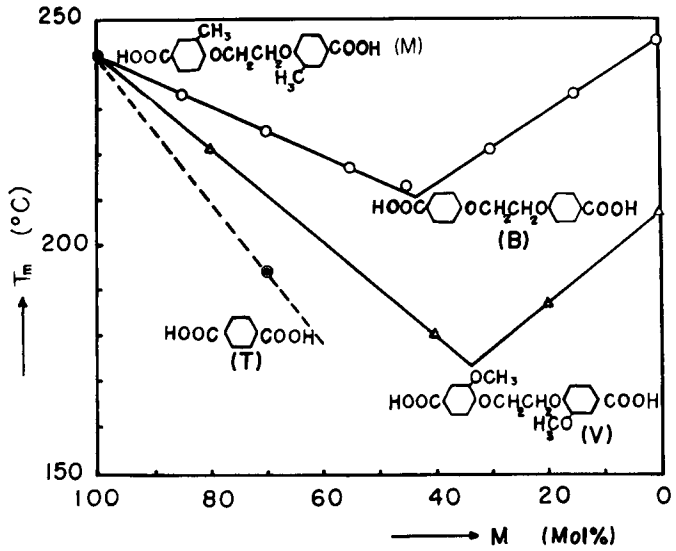

Fig. 45. Melting point vs. composition curves of co-polyesters of polyethylene M-ate/B-ate, M-ate/V-ate and M-ate/terephthalate.

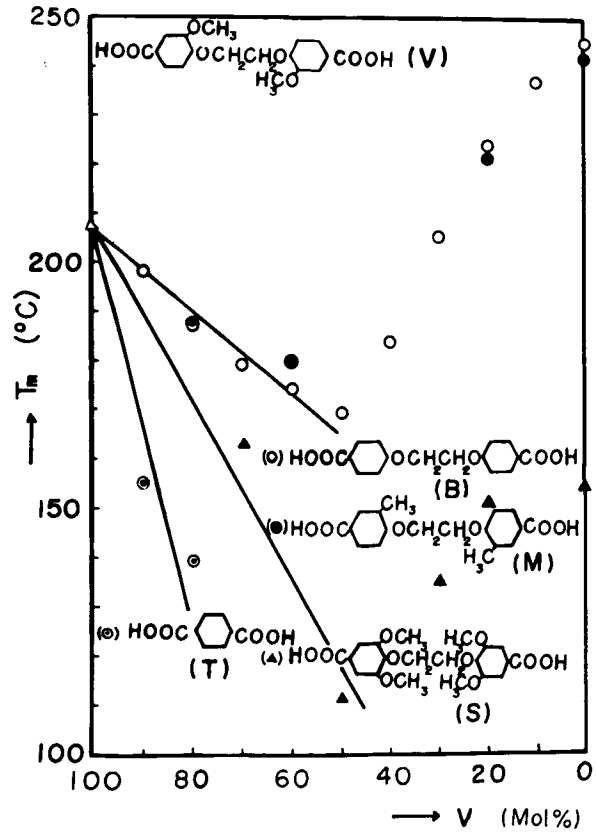

Fig. 46. Melting point vs. composition curves of co-polyesters of polyethylene V-ate/B-ate, V-ate/M-ate, V-ate/S-ate and V-ate/terephthalate.

Fig. 46 shows the melting points of the co-polyesters, that is —polyethylene V-ate/B-ate, polyethylene V-ate/M-ate, polyethylene V-ate/S-ate and polyethylene V-ate/terephthalate. The results are similar to the former cases; the B-ic and M-ic acid ingredients which have greater chemical similarity to the V-ic acid induce the smallest effect upon the melting points of co-polyesters, whilst the terephthalic acid ingredient causes the greatest depression due to the unlikeness of chemical constitution. The fact that S-ic acid ingredient produces a greater depression than B-ic and M-ic acid ingredients can also be readily explained; the S-ic acid has indeed the same skeletal form as V-ic acid, but possesses two excessive methoxyl groups attached to 6 and 6′ positioned carbon atoms of benzene rings and this would prevent the polyethylene V-ate from crystallization.

The x-ray diffraction analyses which were undertaken in parallel offer an interesting information with respect to the structures of co-polyesters, and the results are related to the lowering of melting points and also to the affinity of polymers to each other. The crystal of polyetheylene terephthalate is represented by a triclinic unit cell whose dimension along chain axis is determined to be 10.7A by Daubeny, Bunn and Brown[21]. This value of identity period observed is a little smaller than that calculated under the assumption of fully extended planar chains. The filaments of polyethylene B-ate, polyethylene V-ate and polyethylene M-ate which were cold-drawn up to about six times the original length, also show very distinct x-ray diffraction patterns having the character of fiber diagram. They are given in Figs. 47, 48 and 49,

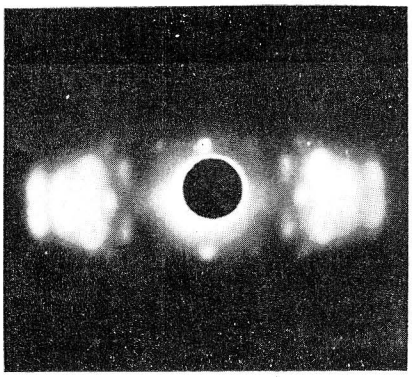

Fig. 47. X-ray diffraction pattern of polyethylene B-ate filaments cold-drawn up to about six times the original length, and thermoset in water at 80°C for 30 min.

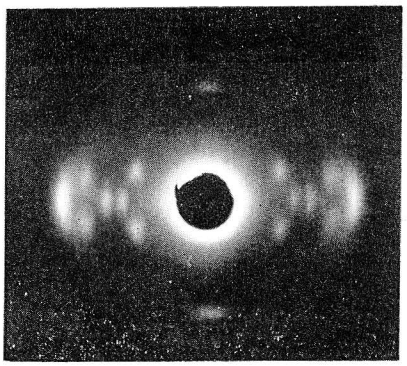

Fig. 48. X-ray diffraction pattern of polyethylene V-ate filaments cold-drawn up to about six times the oniginal length, and thermoset in water at 80°C for 30 min.

which show that these polyesters are highly crystalline and can reach very high orientation of molecules. Only polyethylene S-ate is less crystallizable than the former three polyesters of similar type, as is deduced from its diffraction pattern shown in Fig. 50. This would be due to the abundance of substituents in each benzene ring.

The patterns of the former three polyesters can be analysed by assuming the triclinic unit cells. Polymorphism could be observed with polyethylene B-ate. In this case one of the types is triclinic and the other is orthorhombic. The fiber periods determined from the layer-lines are 18.4 A for polyethylene B-ate, 18.9 A for polyethylene V-ate and 18.6 A for polyethylene M-ate. The fiber period calculated under the assumption of fully extended chains is 19.46 A and therefore, the dimensions observed are somewhat smaller than the calculated value, as is the case with polyethylene terephthalate.

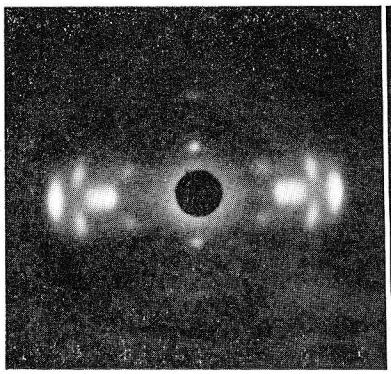

Fig. 49. X-ray diffraction pattern of polyethylene M-ate filaments cold-drawn up to about six times the original length, and thermoset in water at 80°C for 30 min.

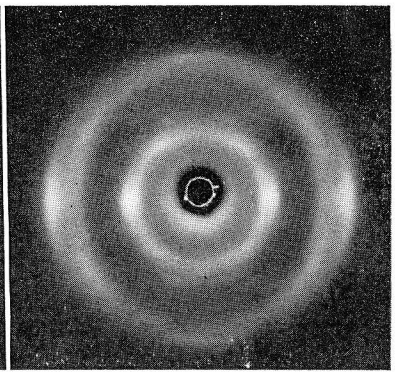

Fig. 50. X-ray diffraction pattern of polyethylene S-ate filaments cold-drawn up to about seven times the original length, and thermoset in water at 70°C for 30 min.

The x-ray diffraction patterns of co-polyesters, that is — polyethylene B-ate/terephthalate and polyethylene B-ate/M-ate, were measured as a function of composition of copolymers. Fig. 51 shows the diffractometer traces of the x-ray diffraction patterns of pure polyethylene B-ate, pure polyethylene terephthalate and the copolymers of polyethylene B-ate 60/terephthalate 40 and polyethylene B-ate 20/terephthalate 80. While each of the homo-polyesters shows very sharp peaks, the patterns of the copolymers are diffused, and both the peaks of polyethylene B-ate and terephthalate decrease in height and increase in width. However, the angles of diffraction of peaks remain unchanged. This means that both the ingredients inhibit with each other from

crystallization, and in consequence the degree of crystallization decreases. Therefore, there is no possibility that both the components participate in the same crystal domain, that is—no possibility of forming the mixed crystals or occurrence of isomorphism. This result is consistent with the remarkable lowering of melting points of co-polyesters consisting of B-yl and terephthalyl components.

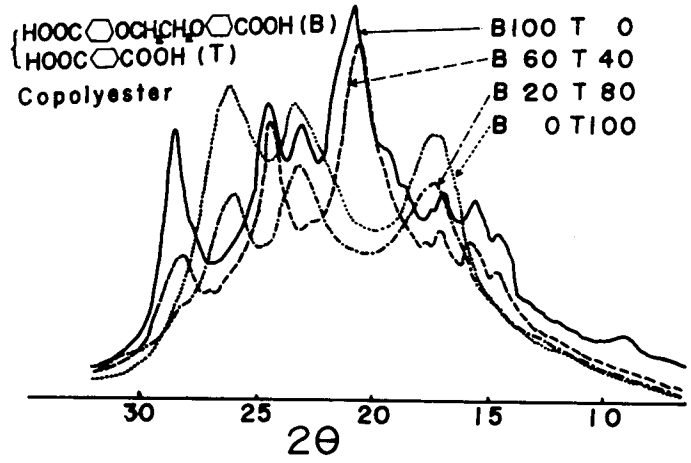

Fig. 51. Diffractometer traces of co-polyesters with the composition of polyethylene B-ate 60/terephthalate 40, B-ate 20/terephthalate 80 and those of homo-polyesters.

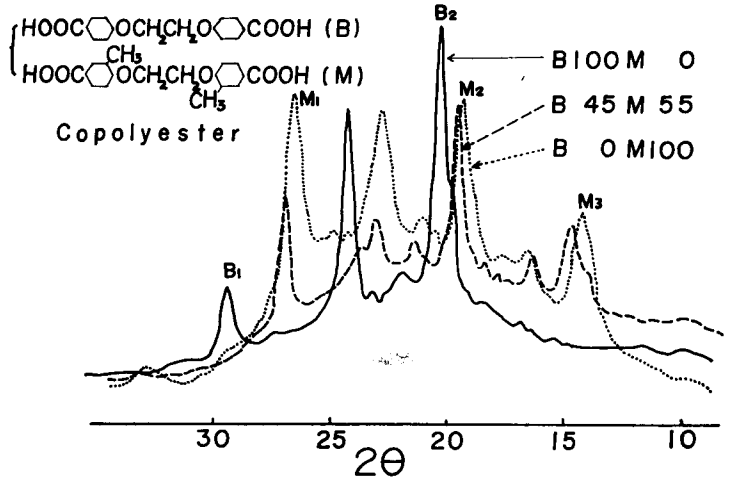

Fig. 52. Diffractometer trace of co-polyester composed of polyethylene B-ate/M-ate, together with that of each homo-polyester.

The relation is considerably different in the case of copolymers consisting of B-yl and M-yl residues. The x-ray diffraction pattern of the copolymer

and those of homopolymers are shown in Fig. 52. The peaks which are assigned to B-component of the copolymers shift towards the smaller angles, that is—the spacings are enlarged under the influence of the coexisting M-component depending upon its content. For example the peak B_1 resulting from B-component is displaced towards the smaller angle with increasing content of M-component. This may be interpreted in another expression that a peak of new spacing appears between B_1 and M_1 instead of them. The spacing corresponding to the peak B_2 is also enlarged by the coexisting M-component and a new peak appears between B_2 and M_2. On the contrary, the peaks which are possibly assigned to M-component shift towards the greater angle, as can be seen with the peaks M_3, that is—the spacings are shortened.

If we consider that the interchain distance of B-polymer would be smaller than that of M-polymer, because of the absence of methyl groups in B-component, it would be natural that the B-lattice is enlarged and the M-lattice is contracted when both the components coexist. In other words, B-component and M-component can have a share in the same crystalline domain, and therefrom arises the possibility of forming isomorphous mixtures or mixed crystals. The smaller depression of melting points of copolymers consisting of these two kindred components of B-ic acid and M-ic acid is interpretable.

We can find the similar relation in the co-polyamides. Edgar and Hill[19] found early that the melting point vs. composition curve of the co-polyamide consisting of hexamethylene adipamide and hexamethylene terephthalamide has no minimum, and the melting point of copolymers rises steadily with increasing content of terephthalyl component. From these experiments they suggested the isomorphous replacement of a part of adipyl residue in polyhexamethylene adipamide by terephthalyl residue as happening. We have measured in this connection the x-ray diffraction of co-polyamides of hexamethylene adipamide/terephthalamide. Fig. 53 shows the diffractometer traces of these co-polyamides. As can be seen in the patterns, the copolymers have a great crystallinity for all the compositions, and this gives an evidence for the existing of isomorphism of the adipyl and terephthalyl residues in copolymers. In this case also the displacement of the diffraction peaks is observed.

The discussion can not be ended without referring to the crystalline state of the blends consisting of two homopolymers. The homo-polyesters of polyethylene B-ate and polyethylene M-ate were dissolved in methyl naphthalene, which is a common solvent of both the polymers, and precipitated by pouring the solution into benzene. The blend specimen was microscopically homogeneous. The x-ray diffractometer trace of the blend is shown in Fig. 54. The pattern is very different from that of copolymer shown in Fig. 52, and is

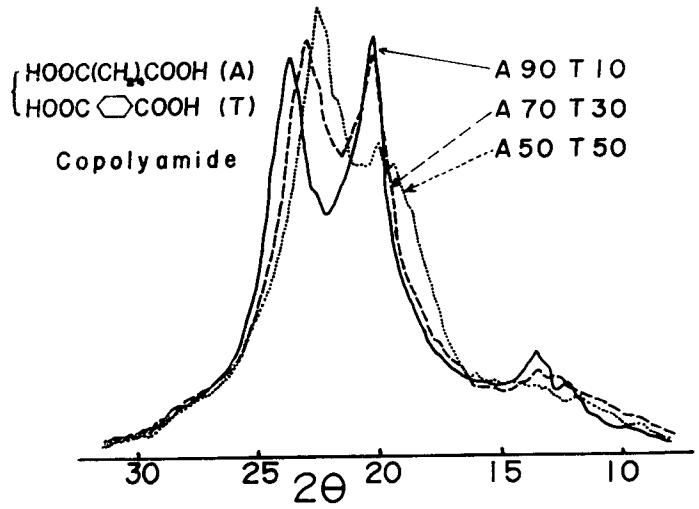

Fig. 53. Diffractometer traces of co-polyamides consisting of polyhexamethylene adipamide/terephthalamide.

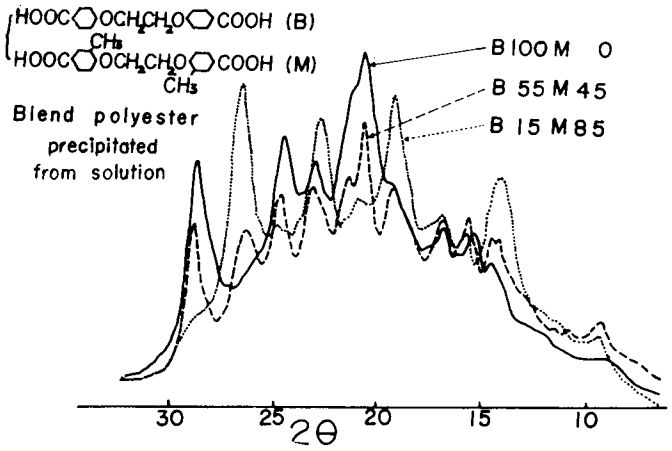

Fig. 54. Diffractometer trace of the precipitate from the mixed solution of polyethylene B-ate and M-ate together with those of homopolyesters.

composed of the peaks characteristic to each of components by the simple additive relation. This means that the precipitate, homogeneous as it may appear macroscopically, consist of isolated crystallites of two homopolymers. The fact that the homopolymers of B- and M-type form mixed crystals can be verified by the experiment as follows: The precipitate mentioned above was molten into a homogeneous melt and cooled down slowly to the room temperature, and then subjected to the diffraction analysis. The diffraction pattern of this specimen is not the same as that observed before melting, but

is similar to that of copolymer, as shown in Fig. 55. This means that B- and M-polymers have a tendency to form the mixed crystals, when the melt of mixture is cooled down slowly.

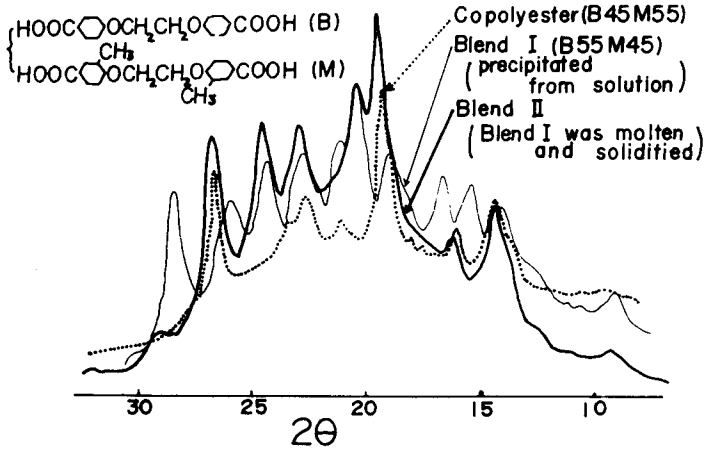

Fig. 55. Diffractometer trace of a specimen prepared as follows: the precipitate from the mixed solution of polyethylene B-ate and M-ate was molten and cooled down to room temperature. The curve of the precipitate before melting (Fig. 54) and that of the co-polyester (Fig. 52) are shown together.

The melting point vs. composition curves of the blends are very different from those of copolymers. Fig. 56 shows the curves of blends and copolymers consisting of polyethylene B-ate and terephthalate. The curve of copolymers has a minimum which lies at a composition about terephthalyl 60/B-yl 40. The minimum melting point is about 170°C and is far below the value of each homopolymers. On the contrary, the minimum is scarecely found in the curve of blend specimens, and the melting point is higher by far than that of copolymer having the same composition of ingredients. In the case of copolymer the residues of the partner component are distributed scattered within each molecular chain and disturb the crystallization most effectively, and this induces the remarkable depression of melting point. In the case of polymer blends of this type, they consist of the crystallites of each component, and the over-all degree of crystallization is high. This results in a higher melting point.

Polyethylene B-ate and polyethylene M-ate have almost the same melting point. They are so intimate that the melting points of blends are almost constant independent of composition, as shown in Fig. 57.

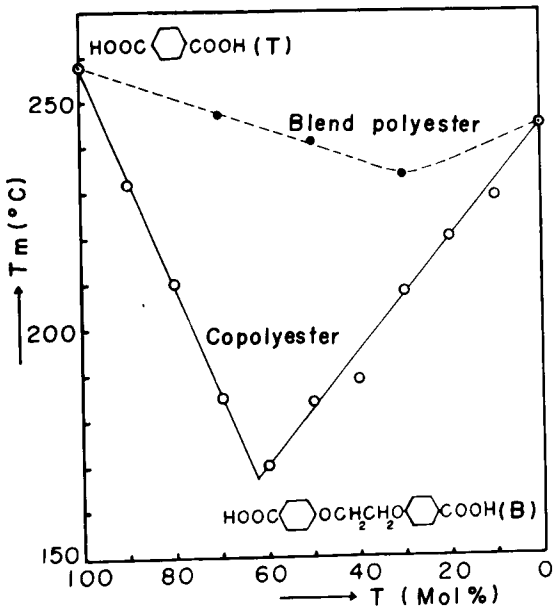

Fig. 56. Melting point vs. composition curve of polymer blends of polyethylene terephthalate/B-ate in comparison with that of copolymers consisting of the same components.

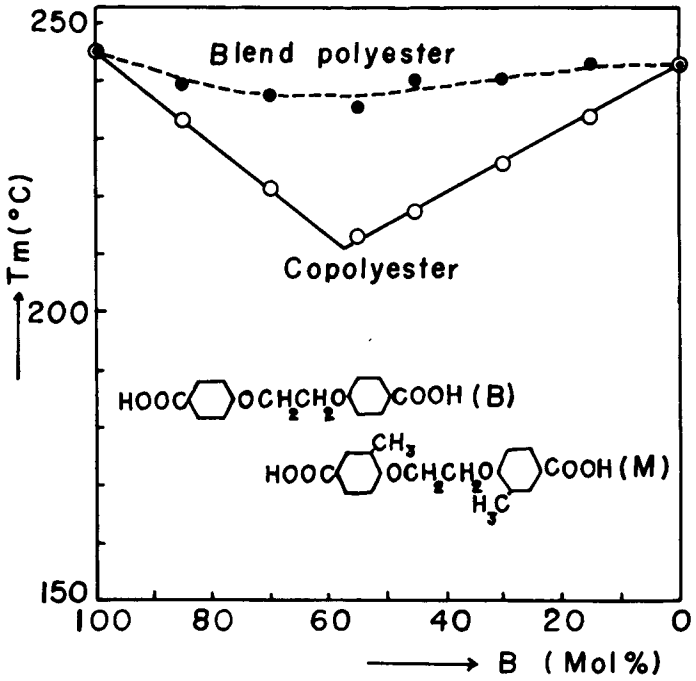

Fig. 57. Melting point vs. composition curve of polymer blends of polyethylene B-ate/M-ate in comparison with that of copolymers consisting of the same components.

Now we are in a position to discuss the interfacial attraction between the crystallites of different polymers in a polymer blend, for example, of polyethylene terephthalate and polyethylene B-ate. The force binding the molecules in the crystals of polyethylene terephthalate is attributed to the van der Waals' force between the chains. This applies also to polyethylene B-ate. Both the chains have the common linking of

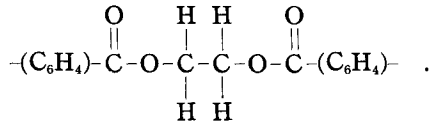

The repetition of this link results in the polyethylene terephthalate. In other words, the strong crystallizing force of polyethylene terephthalate is due to the molecular cohesion of this link. In the case of polyethylene B-ate, the link shown above is intervened by $-OCH_2CH_2O-$, as is demonstrated in Fig. 58. However, this dimensional lag between two types of chains is completely compensated every four units of ethylene B-ate or every seven units of ethylene terephthalate. This means that at every eighth unit of ethylene terephthalate the molecular cohesion similar to that in polyethylene terephthalate comes to action between the two types crystals, when they are arranged in parallel. This suggests that the cohesion between the two types of crystals existing close together would be strong enough.

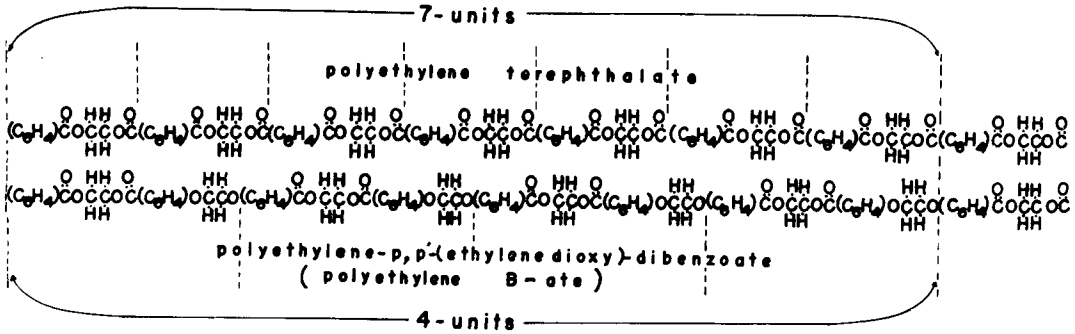

Fig. 58. Comparison between the molecular chains of polyethylene terephthalate and polyethylene B-ate. The lag of dimension between two chains is compensated at every four units of ethylene B-ate or every seven units of ethylene terephthalate.

In the case of the blends of polyethylene B-ate/polyethylene M-ate, the attraction between molecules would be stronger, since the periods of both the molecules are exactly the same, and both the polymers have a tendency to form mixed crystal, as mentioned before.

These conclusions could be evidenced by the production of bilateral fila-

ments of polyethylene terephthalate/B-ate and polyethylene B-ate/M-ate. The cohesion of these components is so strong that every mechanical treatments are unable to separate the filaments into components. Figs. 59 and 60 show the photomicrographs of the bilateral fibers of these types.

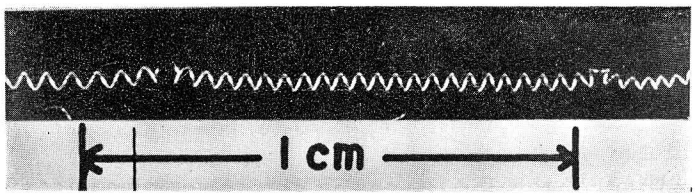

Fig. 59. Conjugate-spun fiber consisting of polyethylene terephthalate and B-ate.

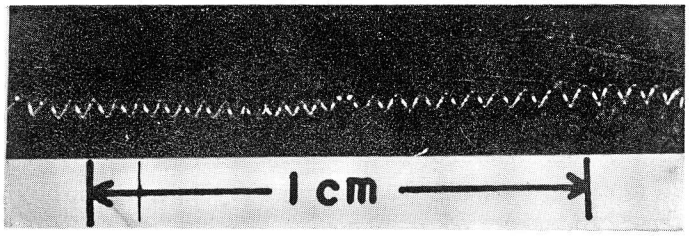

Fig. 60. Conjugate-spun fiber consisting of polyethylene B-ate and M-ate.

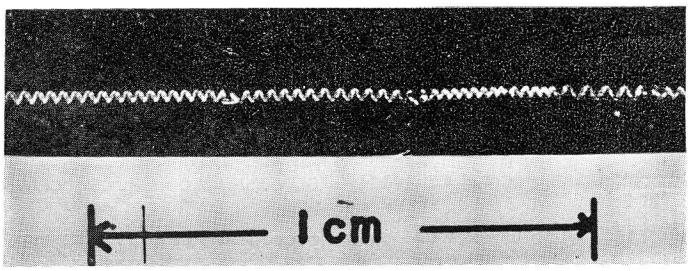

Fig. 61. Conjugate-spun fiber consisting of high density polyethylene and low density polyethylene.

On this occasion we want to refer to the fact that the bilateral fibers having excellent crimp can be obtained with the same substance differing in DP, tacticity and so forth. Beyond dispute these fibers are extremely stable against every mechanical handling. Fig. 61 is the photomicrograph of crimp fiber structured bilaterally with low density polyethylene on one side and high density polyethylene on the other side.

SECTION VII

Effect of the Conditions of Treatment of Conjugate Fibers upon Crimping

The crimp of conjugate-spun fibers depends on the one hand upon the nature of polymers making up each individual fiber, on the other hand upon the conditions of treatment of fibers. Since the coiling results from the difference in the degree of contraction of component polymers, it is necessary in any case that the filament is stretched to a considerable extent to endow it with the property of spontaneous coiling. It can be assumed that the tendency of coiling increases with increasing degree of stretching.

One of the important processes of producing the crimp is the heat treatment. The filament stretched at a certain temperature tends to shrink, when it is heated up to a higher temperature. The difference in the contraction of the two component polymers in a single filament results in the formation of helical spring, whose diameter tends to be smaller as the temperature rises. In Table 6 the features of the crimp are shown as a function of the ratio of stretching at the cold-drawing and the temperature in the heat treatment of the conjugate-spun filaments consisting of nylon 6/nylon 66 in an approximate ratio of 1 : 1.

Table 6. Change in the diameter of helical crimp and the number of crimps per unit length as a function of the ratio of stretching in the cold-drawing and the temperature in the heat treatment in air of the conjugate-spun fibers consisting of nylon 6/nylon 66.

Ratio of stretching (times)	Diameter of fiber (mm)	Temperature in the heat treatment (°C)	Diameter of helix (mm)	Number of crimps per cm
1 (Not stretched)	0.14	180	No crimp	No crimp
3	0.09	No heat treatment	6–10	0.5–1
		100	2– 3	3– 5
		170	1.0–1.5	10–20
4	0.07	No heat treatment	3– 4	3– 4
		100	2.0–2.5	5– 6
		140	1.5–1.7	10–12
		170	0.8–1.0	20–25

The fiber which was not cold-drawn is quite insensitive to heating, and remains almost straight even after the heat treatment at a high temperature. When the fiber is cold-drawn up to three times the original length and released from tension, a very coarse curling is produced, but the fiber may still

be expressed as straight in the practical sense of textiles. This fiber, however, is very sensitive to the heating and tends to form a finely coiled helical spring. The diameter of helix becomes smaller, and consequently the number of crimps per unit length increases with the temperature, as shown in Table 6. The tendency is more distinct in the case of the fiber which was cold-drawn up to four times the original length.

The similar effect of temperature in the heat treatment in air upon the characteristics of crimp can be seen in the conjugate fibers consisting of polyesters, as can be seen in Table 7.

Table 7. Effect of the temperature in the heat treatment in air upon the character of the crimp of conjugate fibers consisting of polyesters whose molar ratio is about 1 : 1.

Components	Diameter of fiber (mm)	Ratio of stretching (times)	Temperature at stretching (°C)	Temperature in the heat treatment (°C)	Diameter of helix (mm)	Number of crimps per cm
PET* PET-PEI**	0.08	4.8	80	90	2.0	20
				100	0.8	60
				170	0.5	110
PET-PEI PET-PEI $+TiO_2$***	0.05	5.6	80	110	2.5	10
				150	1.5	20
				170	0.8	50
High DP PET Low DP PET	0.05	5.0	80	100	2.0	5
				130	1.2	16
				170	0.9	45

* Polyethylene terephthalate,

** Copolymer of polyethylene terephthalate and polyethylene isophthalate 90 : 10 in molar ratio,

*** The above copolymer mixed with TiO_2 1% in weight.

Table 8. Production of crimps by the treatment of conjugate fibers consisting of polyester components with aqueous solution of phenol.

Ratio of stretching (times)	Diameter of fiber (mm)	Medium of treatment	Temperature of treatment (°C)	Diameter of helix (mm)	Number of crimps per cm
4.8	0.05	Air	80	1.8-2.2	15- 20
		"	100	0.8-1.2	50- 70
		"	170	0.4-0.5	100-200
		Water	100	0.5-0.8	60- 80
		5% aq. phenol	25	1.5-1.6	50- 70
		5% aq. phenol	80	1.0	80-100

The practical method of producing crimps other than by the heat treatment consists in the application of swelling agents at lower temperature. It is shown in Table 8 that the aqueous solution of phenol is effective to produce crimping of conjugate fibers consisting of polyethylene terephthalate/polyethylene terephthalate-isophthalate.

Acknowledgments

The author is indebted to Professors T. Kondo and S. Nagata, and Messrs. K. Sekimoto, M. Funatsu and S. Murakami for their collaboration and help in the work of crimped rayon staple and crimp of wool fibers, and to Professor K. Kobayashi and Mr. T. Takahashi for their collaboration in the work of oriented overgrowth, and to Professors R. Imamura and T. Kondo, and Dr. T. Kiotsukuri, and Messrs. K. Sekimoto and S. Nomachi for their co-operation in the work of the conjugate spinning and related matters.

Thanks are also due to the financial support by the grant from the scientific research funds (Kagaku Kenkyu-hi) of the Ministry of Education, Japan, the grant from the Research Institute for Synthetic Fibers, Japan, and the grant from the International Wool Secretariat, London.

Literature

1) M. Horio and T. Kondo, Textile Res. J., **23**, 137 (1953).
2) M. Horio and T. Kondo, Textile Res. J., **23**, 373 (1953).
3) K. Ohara, Melliand Textilber., **19**, 407 (1938).
4) M. Horio, T. Kondo, K. Sekimoto and A. Teramoto, Zeitschr. f. Naturforsch., **15**, 343 (1960).
5) J. Dusenbury and A. B. Coe, Textile Res. J., **25**, 354 (1955).
6) J. Meybeck, Proc. Int. Wool Textile Res. Conf., Australia, Volume F, 217 (1955).
7) M. Leveau, A. Parisot and N. Cebe, Bull. de Institut Textile de France, **43**, 33 (1953).
8) A. Pischinger, Zeitschr. Zellforsch. Mikrop. Anatom., **3**, 169 (1926).
9) L. Lison, "Histochimie et Cytochimie Animales". Gauthier-Villars, Paris (1953).
10) Proc. Int. Wool Textile Res. Conf., Australia, Volume F, 225 (1955) : Discussion on Nomenclature to be Used for the Two Segments or Types of Cortical Cells in Wool.
11) E. G. Bendit, J. Textile Inst., T544 (1960).
12) T. Kondo, Collection of Papers of Res. Inst. Synthetic Fibers, Japan, **12**, 98 (1955).
13) E. M. Hicks, J. F. Ryan, R. B. Taylor and R. L. Tichenor, Textile Res. J., **30**, 675 (1960).
14) J. Willems, Experimentia, **13**, 465 (1957) ; Trans. Farad. Soc., General Discussion, **25-26**, 111 (1958).
15) R. Eppe, E. W. Fischer and H. A. Stuart, J. Polym. Sci., **34**, 721 (1959).
16) E. W. Fischer, Trans. Farad. Soc., General Discussion, **25-26**, 204 (1958).
17) R. B. Richards, J. Polym. Sci., **6**, 397 (1951).
18) J. Willems and I. Willems, Naturwiss., 429 (1956).
19) O. B. Edgar and R. Hill, J. Polym. Sci., **8**, 1 (1951).
20) P. J. Flory, J. Chem. Phys., **17**, 223 (1949).
21) R. P. Daubeny, C. W. Bunn and C. J. Brown, Proc. Royal Soc., **A226**, 531 (1954).